Discovery of an embryonically derived bipotent population of endothelial-macrophage progenitor cells in postnatal aorta

Running title: Embryonically derived aortic endothelial-macrophage progenitors

Anna E. Williamson[1,2 †], Sanuri Liyanage[1,2†], Mohammadhossein Hassanshahi[1,2], Malathi S.I. Dona[3], Deborah Toledo-Flores[1], Dang X.A. Tran[1], Catherine Dimasi[1], Nisha Schwarz[1], Sanuja Fernando[1,2], Thalia Salagaras[1], Aaron Long[1,4], Jan Kazenwadel[5], Natasha L. Harvey[2,5], Grant R. Drummond[6], Antony Vinh[6], Vashe Chandrakanthan[2,7,8], Ashish Misra[9], Zoltan Neufeld[10], Joanne T.M. Tan[1,2], Luciano Martelotto[11], Jose M. Polo[11], Claudine S. Bonder[5], Alexander R. Pinto[3,6], Shiwani Sharma[1,12], Stephen J. Nicholls[13], Christina A. Bursill[1,2], Peter J. Psaltis[1,2, 4 *]

[1] Vascular Research Centre, Heart and Vascular Program, Lifelong Health Theme, South Australian Health and Medical Research Institute, Adelaide, South Australia, 5000 Australia

[2] Adelaide Medical School, Faculty of Health and Medical Sciences, The University of Adelaide, Adelaide, South Australia, 5000, Australia

[3] Cardiac Cellular Systems Laboratory, Baker Heart and Diabetes Institute, Melbourne, Victoria, 3004, Australia.

[4] Department of Cardiology, Royal Adelaide Hospital, Central Adelaide Local Health Network, Adelaide, South Australia, 5000, Australia

[5] Centre for Cancer Biology, University of South Australia and SA Pathology, Adelaide, South Australia, 5000, Australia

[6] Department of Microbiology, Anatomy, Physiology and Pharmacology and Centre for Cardiovascular Biology and Disease Research, School of Agriculture, Biomedicine and Environment, La Trobe University, Bundoora, Victoria, 3086, Australia.

[7] School of Medical Sciences, University of New South Wales, Sydney, New South Wales, 2052, Australia

[8] Precision Medicine, South Australian Health and Medical Research Institute, Adelaide, South Australia, 5000, Australia

[9] Faculty of Medicine and Health, University of Sydney and Heart Research Institute, Newtown, New South Wales, 2042, Australia

[10] School of Mathematics and Physics, The University of Queensland, Brisbane, Queensland, 4072, Australia

[11] Adelaide Centre for Epigenetics and the South Australian Immunogenomics Cancer Institute, Faculty of Health and Medical Sciences, The University of Adelaide, Adelaide, SA 5000, Australia

[12] Flinders Medical Research Institute, College of Medicine and Public Health, Flinders University, Bedford Park, SA 5042, Australia

[13] Monash Cardiovascular Research Centre, Monash University, Clayton, Melbourne, Victoria, 3800, Australia

[†] These authors contributed equally: Anna E. Williamson and Sanuri Liyanage.

* corresponding author

SUPPLEMENTARY TABLES

Experimental Design	**Matrigel™** ***In vitro***	**Aortic Ring** ***Ex vivo***	**Hindlimb** ***In vivo***
Surface marker	**$CD45^+CD11b^+F4/80^+$ Macrophages**		
$CD206^+$	75.8 ± 23.9% (*n*=5)	85.1 ± 20.6% (*n*=3)	68.4 ± 17.0% (*n*=6)
CX_3CR1^+	74.5 ± 16.3% (*n*=5)	90.9 ± 13.4% (*n*=3)	91.0 ± 8.7% (*n*=6)
MHC II^+	5.8 ± 2.5% (*n*=4)	2.9 ± 0.0% (*n*=2)	19.4 ± 7.2% (*n*=3)
LYVE-1^+	45.0 ± 21.4% (*n*=6)	83.9 ± 0.8% (*n*=2)	61.2 ± 16.5% (*n*=6)
$CCR2^+$	5.5 ± 4.1% (*n*=4)	N.D.	27.6 ±1.9% (*n*=3)
	$CD45^-CD31^+$ and/or $CD45^-CDH5^+$ Endothelial cells		
$VEGFR2^+$	40.0 ± 13.3% (*n*=6)	23.6 ± 0.8% (*n*=2)	77.9 ± 19.4% (*n*=6)
$TIE2^+$	80.4 ± 3.9% (*n*=3)	N.D.	N.D.

Supplementary Table 1. Sub-lineage marker expression of cells produced by aortic EndoMac progenitors in different experimental models.

Expression of select surface markers on macrophages and endothelial cells produced by adult aortic progenitors in Matrigel™ cord-forming assay, aortic ring assay and after intramuscular injection in hindlimb ischemia model. *n*-values relate to number of experiments in which these markers were assessed. N.D., not determined. Results are summarized as mean ± standard deviation. Also see Fig. 4, 5 and Supplementary Fig. 8, 10.

	Sequencing run 1	Sequencing run 2	Combined output from two runs
Estimated Number of Cells	29,539	32,789	34,813
Mean Reads per Cell	14,912	48,013	54,874
Median Genes per Cell	2,306	3,427	3,534
Number of reads	440,473,799	1,574,282,809	2,014,756,608
Sequencing saturation	25.3%	54.5%	60.3%
Fraction reads in cell	90.2%	93.1%	95.2%
Total genes detected	25,482	26,164	26,617
Median UMI counts per cell	6,399	12,426	13,116

Supplementary Table 2. Cell Ranger summary statistics for scRNA-seq runs.

Two sequencing runs were performed to achieve ~50,000 mean reads per cell.

Cell cluster	Number of cells
Progenitors1	1,558
Progenitors2	1,510
Progenitors3	1,130
Progenitors4	1,126
Progenitors5	775
Progenitors6	262
Progenitors7	133
Prolif.Progenitors1	950
Prolif.Progenitors2	522

Supplementary Table 3. Numbers of cells contained within aortic CFU-M progenitor cell clusters identified by scRNA-seq.

SUPPLEMENTARY FIGURES

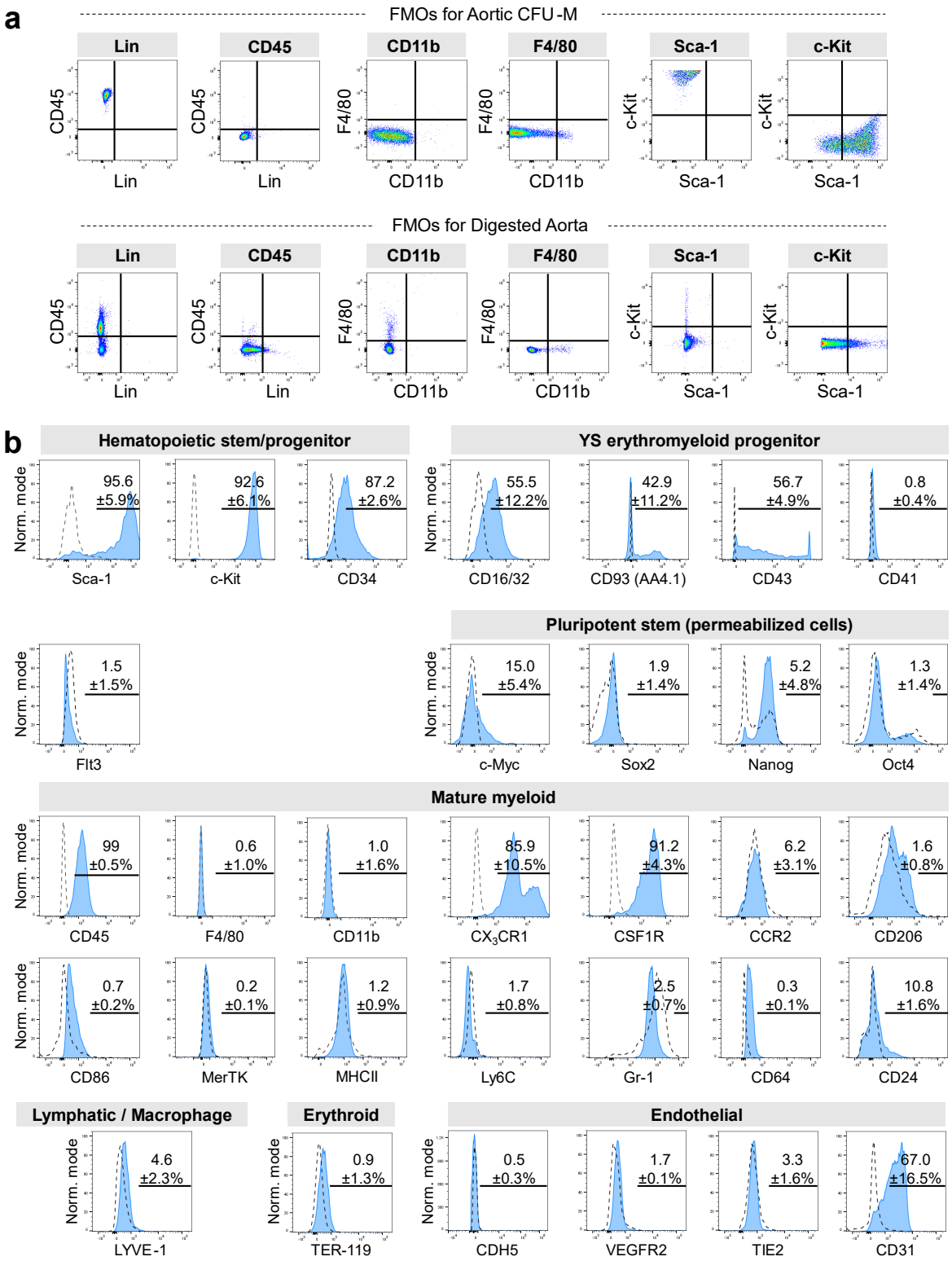

Supplementary Fig. 1. Surface marker expression of progenitors contained within 1° aortic CFU-M.

(a) Top row: Fluorescence-minus-one (FMO) controls for flow cytometry performed on cells from medium-sized aortic CFU-M in Fig. 1c and d. Bottom row: FMO controls used for flow cytometry performed on cells from aortic digests in Fig. 1e.

(b) Flow cytometry histograms show expression of different surface markers on cells from medium-sized 1° aortic CFU-M (blue histogram) from 12 w C57BL/6J mice ($n \geq 3$). Dotted histogram, FMO control. YS, yolk sac. Mean ± SD of % expression values are shown.

Also see Fig. 1. Source data are provided as a Source Data file.

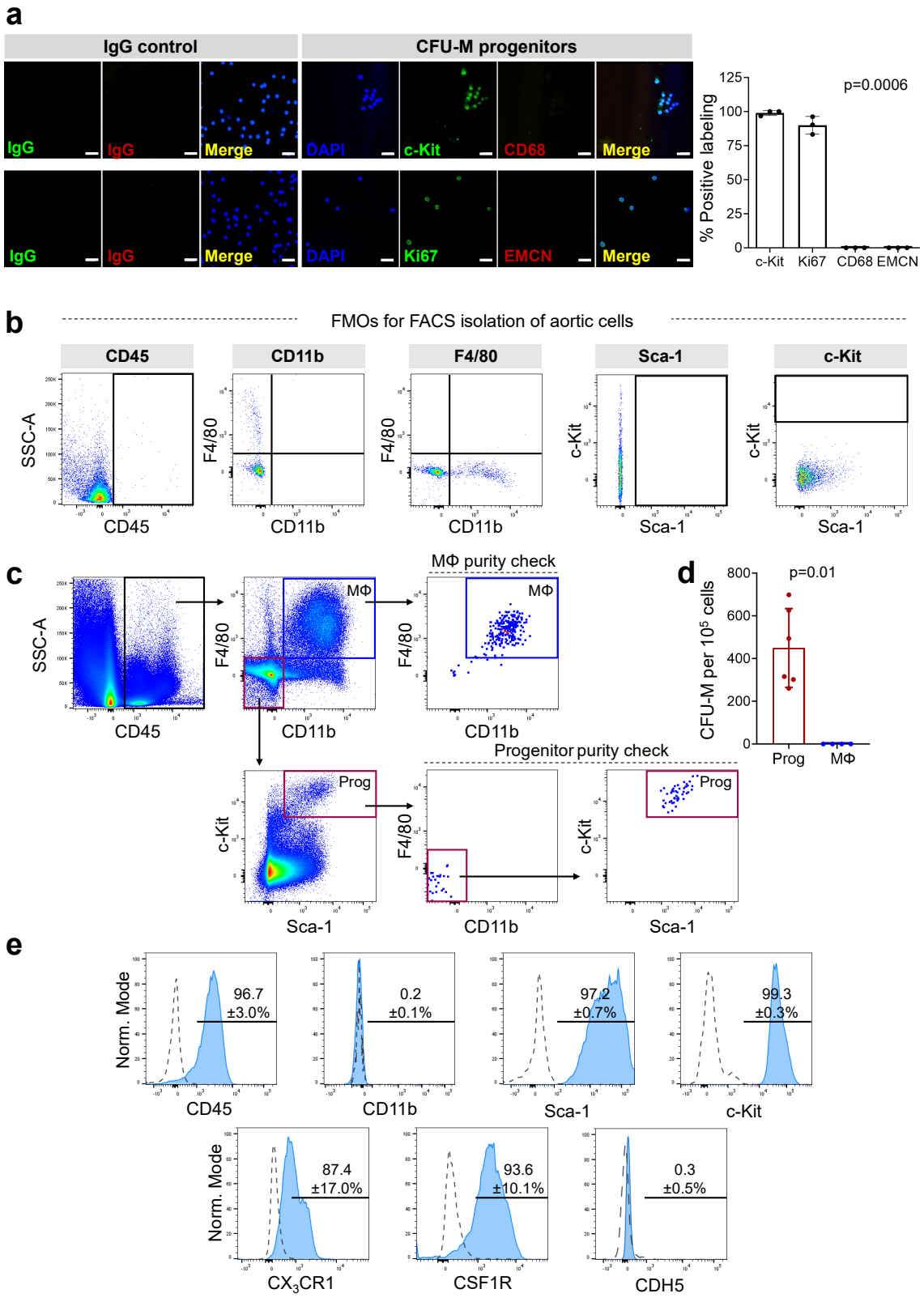

Supplementary Fig. 2. Immunophenotypic confirmation of cell population responsible for aortic CFU-M.

(a) Confocal microscopy images of immunofluorescence labeled cytospin preparations of cells from aortic CFU-M. Scale bar, 100μm. Graph summarizes % of positively labeled cells with each marker. Data from three separate experiments using CFU-M from adult C57BL/6J aorta from different mice were analyzed by Kruskal-Wallis test without multiple comparisons test.

(b) Fluorescence-minus-one (FMO) controls used for fluorescence assisted cell sorting (FACS) to isolate progenitors (Prog) and macrophages (MΦ) from aortic cells of adult C57BL/6J mice.

(c) Representative flow cytometry dot plots used to FACS-isolate progenitors and macrophages from aorta, with purity checks of sorted populations.

(d) Graph summarizes CFU-M yield from sorted aortic cell populations. $n = 6$ (prog) and $n = 4$ (MΦ) independent experiments each using aortas from ≥ 6 mice. Data was analyzed using two-tailed Mann-Whitney U test.

(e) Flow cytometry histograms showing surface marker expression of cells contained in CFU-M produced by sorted aortic progenitors (blue histograms). Dotted histograms, FMO controls. $n = 3$ mice.

Data summarized as mean ± SD.

Also see Fig. 1. Source data are provided as a Source Data file.

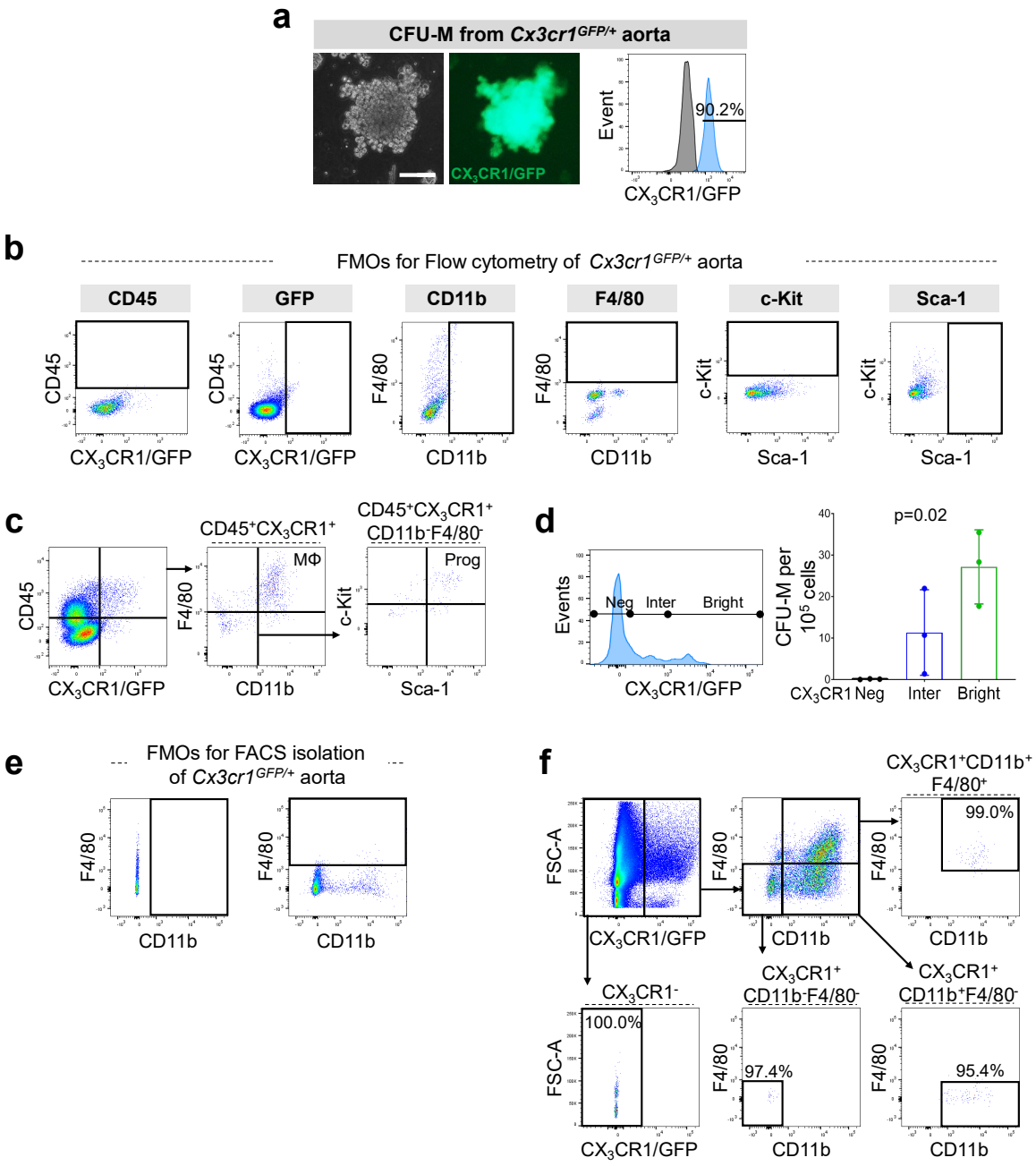

Supplementary Fig. 3. Aortic CFU-M progenitors express CX₃CR1.

(a) Light and fluorescence microscopy and flow cytometry (blue histogram) show GFP$^+$ (CX_3CR1^+) expression of cells contained in CFU-M from 12 w *Cx3cr1*$^{GFP/+}$ aortas. Gray histogram, C57BL/6J control. $n = 1$. Scale bar, 100 µm.

(b) Fluorescence-minus-one (FMO) controls used for flow cytometry analysis of aortic digests from *Cx3cr1*$^{GFP/+}$ mice.

(c) Flow cytometry showing presence of $CD11b^{-}F4/80^{-}Sca\text{-}1^{+}c\text{-}Kit^{+}$ progenitors (Prog) and $CD11b^{+}F4/80^{+}$ macrophages (MΦ) among $CD45^{+}CX_3CR1^{+}$ cells in aortas of 12 w *Cx3cr1*$^{GFP/+}$ mice. Representative of $n = 6$ mice.

(d) Fluorescence assisted cell sorting (FACS)-isolation of CX_3CR1^{Neg}, CX_3CR1^{inter} and CX_3CR1^{bright} populations from 12 w *Cx3cr1*$^{GFP/+}$ aortas. Graph shows 1° CFU-M yield from each population ($n = 3$ experiments, with six aortas each; repeated measures one-way ANOVA with Tukey's multiple comparisons test). Neg, negative; Inter, intermediate.

(e) FMO controls used for FACS-isolation of aortic cells from *Cx3cr1*$^{GFP/+}$ mice.

(f) Gating strategy and purity checks for FACS-isolation of aortic cells from 12 w *Cx3cr1*$^{GFP/+}$ mice into $CX_3CR1^{+}CD11b^{-}F4/80^{-}$, $CX_3CR1^{+}CD11b^{+}F4/80^{+}$, $CX_3CR1^{+}CD11b^{+}F4/80^{-}$ and CX_3CR1^{-} populations, used in Fig. 1h.

Data summarized as mean ± SD.

Also see Fig. 1. Source data are provided as a Source Data file.

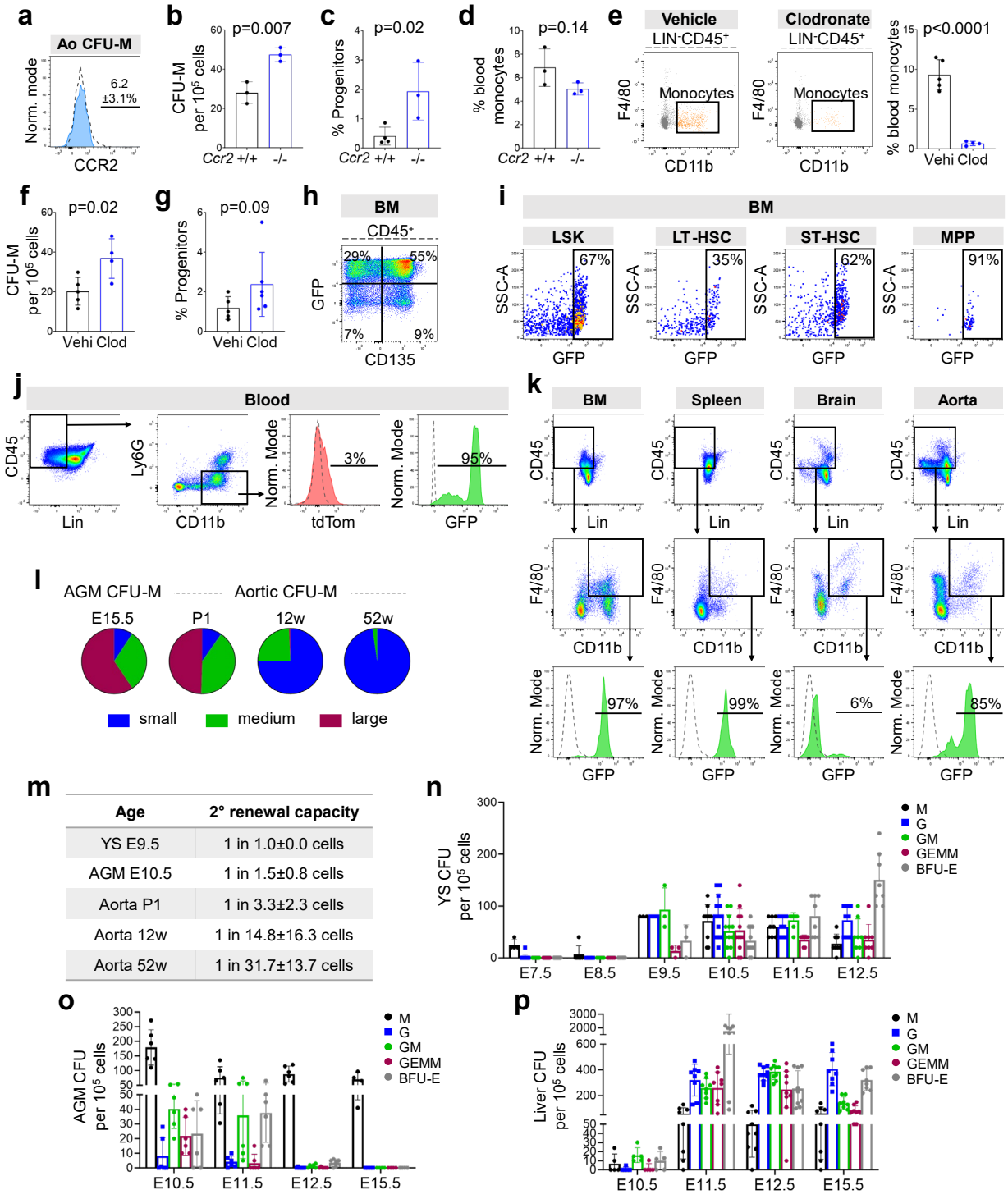

Age	2° renewal capacity
YS E9.5	1 in 1.0±0.0 cells
AGM E10.5	1 in 1.5±0.8 cells
Aorta P1	1 in 3.3±2.3 cells
Aorta 12w	1 in 14.8±16.3 cells
Aorta 52w	1 in 31.7±13.7 cells

Supplementary Fig. 4. Origins of CFU-M.

(a) Surface expression of CCR2 on progenitor cells from 1° aortic (Ao) CFU-M (blue histogram). Dotted histogram, fluorescence-minus-one (FMO) control. *n* = 3 mice.

(b-d) Graphs show comparisons of (b) CFU-M yield and percentage of (c) progenitors in

aorta, and (d) blood monocytes between 12 w *Ccr2*$^{+/+}$ and *Ccr2*$^{-/-}$ mice, measured by flow cytometry (n = 3; two-tailed unpaired t-tests).

(e-g) Flow cytometry plots and graphs show comparisons of percentage of (e) blood monocytes, and (g) progenitors and (f) CFU-M yield in aorta of 12 w C57BL/6J mice following clodronate (Clod) or vehicle (Vehi) ($n \geq 4$) treatment. Two-tailed, unpaired t-tests (e, f) and Mann-Whitney U test (g).

(h) Flow cytometry plot showing correlation of CD135 (Flt3) and green fluorescent protein (GFP) expression in CD45$^+$ cells in bone marrow (BM) of adult *Flt3*^{Cre} x *Rosa*^{mTmG} mice (n = 5).

(i-j) Flow cytometry plots and histograms show GFP$^+$ (Flt3-Cre$^+$) status of (i) BM long-term (LT) and short-term (ST) HSCs, multipotent progenitors (MPP) and (j) blood monocytes from adult *Flt3*^{Cre} x *Rosa*^{mTmG} mice. Percentages represent mean of $n \geq 5$. Dotted histograms, C57BL/6J control. LSK, Lin$^-$Sca-1$^+$c-Kit$^-$. tdTom, tdTomato. *Please see Source Data file for FMO controls and gating strategy for BM, and Methods for immunophenotypic definitions of BM cell populations*.

(k) Flow cytometry of GFP$^+$ (Flt3-Cre$^+$) expression on macrophages from different tissues of adult *Flt3*^{Cre} x *Rosa*^{mTmG} mice. Green histogram, sample; dotted histogram, control. Percentages are mean % GFP$^+$ cells from n = 4 mice.

(l) Pie charts show classification of CFU-M by colony size from E15.5 aorta-gonad-mesonephros (AGM), and aorta at different postnatal ages from C57BL/6J mice. E15.5: 4, P1: 3, 12 w: 5 and 52 w: 4 mice.

(m) Frequency of self-renewal of progenitor cells from 1° CFU-M from yolk sac (YS), AGM and aorta at different ages, expressed as a 2° CFU-M generated per individually seeded cells. YS E9.5: 3, AGM E10.5: 4, P1: 14, 12 w: 20 and 52 w: 4 replicates.

(n-p) Frequency of CFU types from (n) YS (o) AGM and (p) liver at different embryonic ages of C57BL/6J mice. YS - E7.5 and E10.5: 12, E8.5: 1, E9.5: 3 and E11.5 and E12.5: 8 embryos; AGM - E10.5, E11.5 and E12.5: 6 and E15.5: 4 embryos; liver - E10.5: 5, E11.5 and E15.5: 8 and E12.5: 9 embryos. M, macrophage; G, granulocyte; GM, granulocyte-macrophage; GEMM, granulocyte-erythrocyte-monocyte-megakaryocyte; BFU-E, burst-forming units-erythroid.

Data summarized as mean or mean ± SD.

Also see Fig. 2. Source data are provided as a Source Data file.

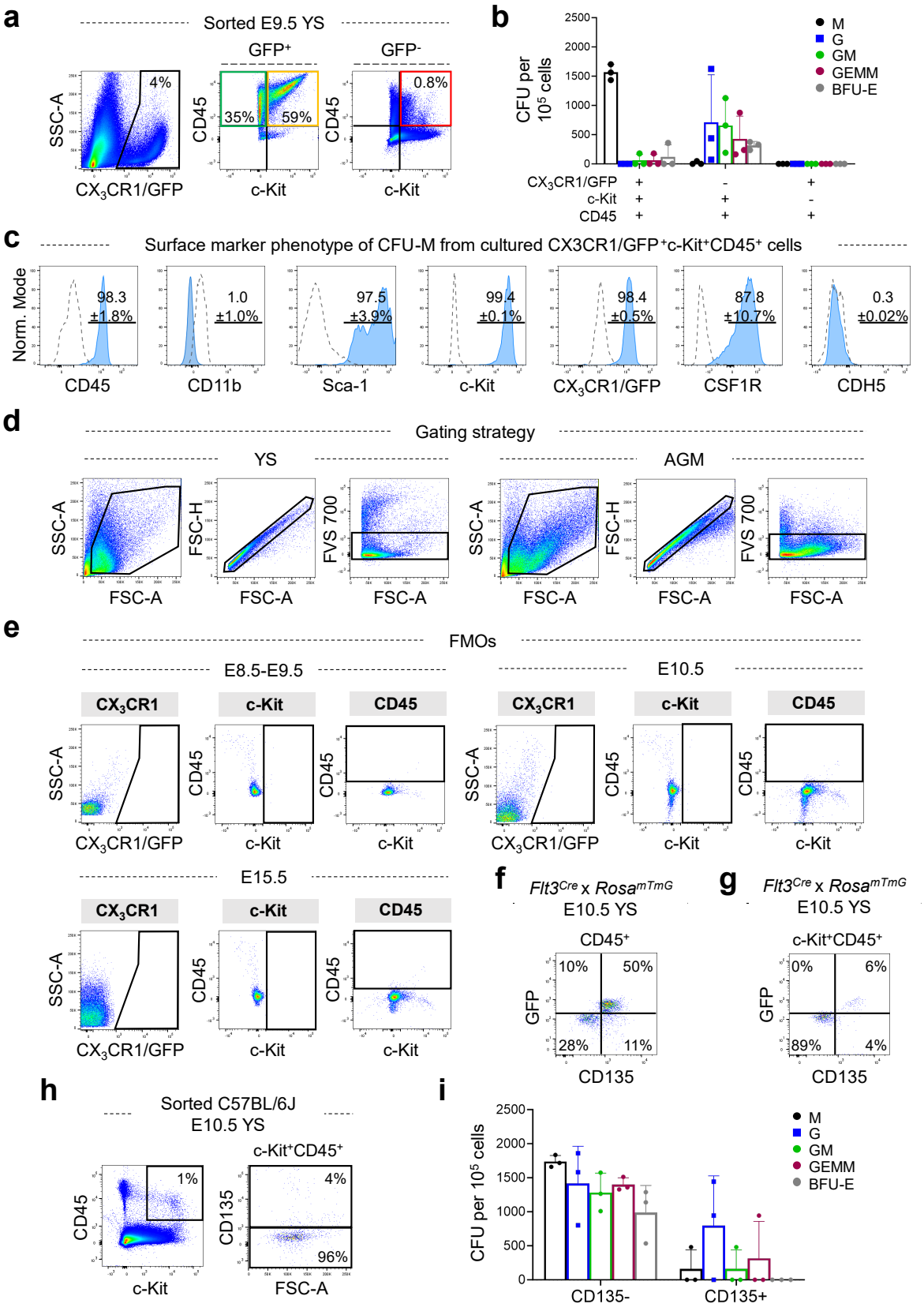

Supplementary Fig. 5. Identification of CFU-M progenitors in E9.5 Yolk Sac.

(a) Gating strategy for fluorescence assisted cell sorting (FACS)-isolation of yolk sac (YS) cells from E9.5 *Cx3cr1*$^{GFP/+}$ embryos into CX_3CR1/GFP^+c-Kit^+CD45^+ (yellow box), CX_3CR1/GFP^+c-Kit^-CD45^+ (green box) and CX_3CR1/GFP^-c-Kit^+CD45^+ (red box) populations, used in Fig. 2h. Percentages are from the parent population of the example shown.

(b) Yield of different types of colonies from the FACS-isolated populations. $n = 3$ experiments. Also see Fig. 2g. M, macrophage; G, granulocyte; GM, granulocyte-macrophage; GEMM, granulocyte-erythrocyte-monocyte-megakaryocyte; BFU-E, burst-forming units-erythroid.

(c) Flow cytometry histograms showing surface expression of markers (blue histograms) on cells contained in CFU-M produced by sorted YS progenitors. Dotted histograms, fluorescence-minus-one (FMO) controls. Percentages represent mean of $n = 4$ experiments, performed using pooled tissue from one litter each.

(d) Gating strategy used for flow cytometry of YS and aorta-gonad-mesonephros (AGM) cells from *Cx3cr1*$^{GFP/+}$ embryos shown in Fig. 2i and j.

(e) FMO controls used for flow cytometry of YS and AGM, and FACS-isolation of YS cells from *Cx3cr1*$^{GFP/+}$ embryos in Fig. 2h and 2i and Supplementary Fig. 5a.

(f-g) Flow cytometry plots showing correlation of CD135 (Flt3) and green fluorescent protein (GFP) expression in (f) $CD45^+$ and (g) c-Kit^+CD45^+ cells in E10.5 YS from *Flt3*^{Cre} x *Rosa*^{mTmG} embryos ($n = 5$ embryos).

(h) Gating strategy used for FACS-isolation of c-$Kit^+CD45^+CD135^-$ and c-$Kit^+CD45^+CD135^+$ cells from E10.5 YS from C57BL/6J embryos. Percentages are from the parent population of the example shown.

(i) Graph summarizes the yield of different types of colonies formed from the two FACS-isolated cell populations (n = 3 pools, each consisting of tissue from a minimum of 4 and up to 10 embryos from more than one litter).

Data summarized as mean or mean ± SD.

Also see Fig. 2. Source data are provided as a Source Data file.

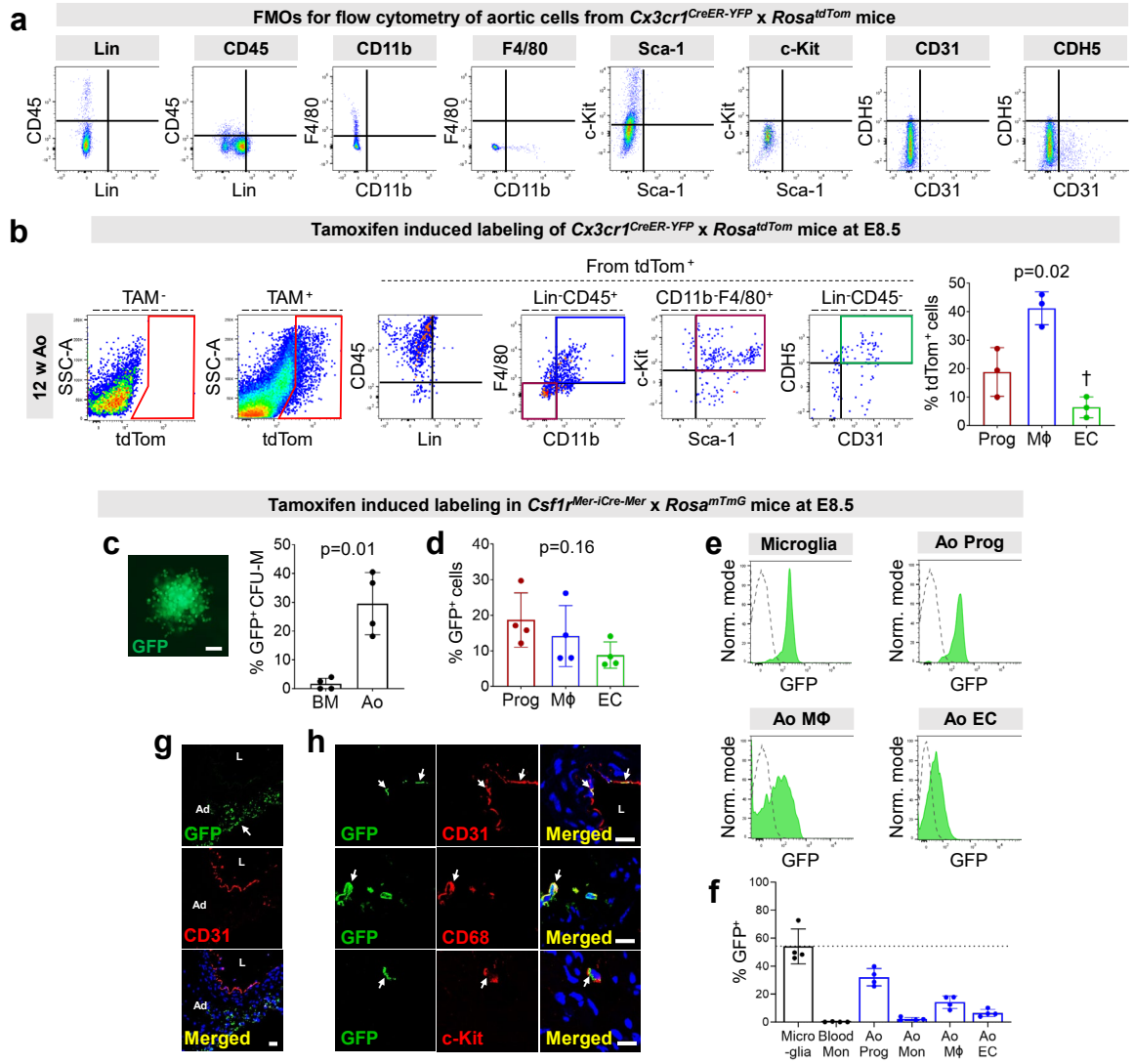

Supplementary Fig. 6. Aortic CFU-M progenitors arise from CX3CR1+ and CSF1R+ cells in the early embryo.

(a) Fluorescence-minus-one (FMO) control staining used to analyze cells from E15.5 aorta-gonad-mesonephros (AGM) and adult aorta from *Cx3cr1*$^{CreER\text{-}YFP}$ x *Rosa*^{tdTom} mice, shown in Fig. 3c and d.

(b) Flow cytometry dot plots showing composition of tdTomato positive (tdTom^{+}) cells in 12 w adult aortas of *Cx3cr1*$^{CreER\text{-}YFP}$ x *Rosa*^{tdTom} mice following *in utero* induction with tamoxifen (TAM) at E8.5. Gated regions correspond to macrophages (Mϕ, blue), progenitors (Prog, maroon) and endothelial cells (EC, green). tdTom expression from aorta of no TAM

(TAM$^-$) control is also shown. Graph shows the % of tdTom$^+$ cells that comprised each of these three cell populations (n = 3 mice). Data was analyzed using repeated measures one-way ANOVA with Tukey's multiple comparisons test. †Adjusted p = 0.003 vs Mϕ.

(c-h) *Csf1r*$^{Mer\text{-}iCre\text{-}Mer}$ x *Rosa*^{mTmG} mice were induced with TAM at E8.5 and analyzed at 12 w.

(c) Image of GFP$^+$ CFU-M from 12 w aorta. Graph shows % GFP$^+$ CFU-M from aorta (Ao) and bone marrow (BM) (n = 4 mice; two-tailed paired t-test).

(d) Graph summarizes % breakdown of GFP$^+$ cells in adult aorta (n = 4 mice; repeated measures one-way ANOVA with Tukey's multiple comparisons test).

(e, f) Histograms and graph showing % GFP expression in different cell populations from brain and aorta of 12 w mice (n = 4 mice). Green histogram, sample; dotted histogram, TAM$^-$ control.

(g, h) Confocal microscopy of immunolabeled sections of 12 w aorta shows (g) GFP$^+$ cells in adventitia (Ad), with (h) magnified examples of GFP$^+$ cells expressing CD31 in the intima, and CD68 and c-Kit in adventitia (arrows). Data representative of three mice. L, lumen.

Data summarized as mean ± SD. Scale bar, 100 μm in (a) and 20 μm in (g, h).

Also see Fig. 3. Source data are provided as a Source Data file.

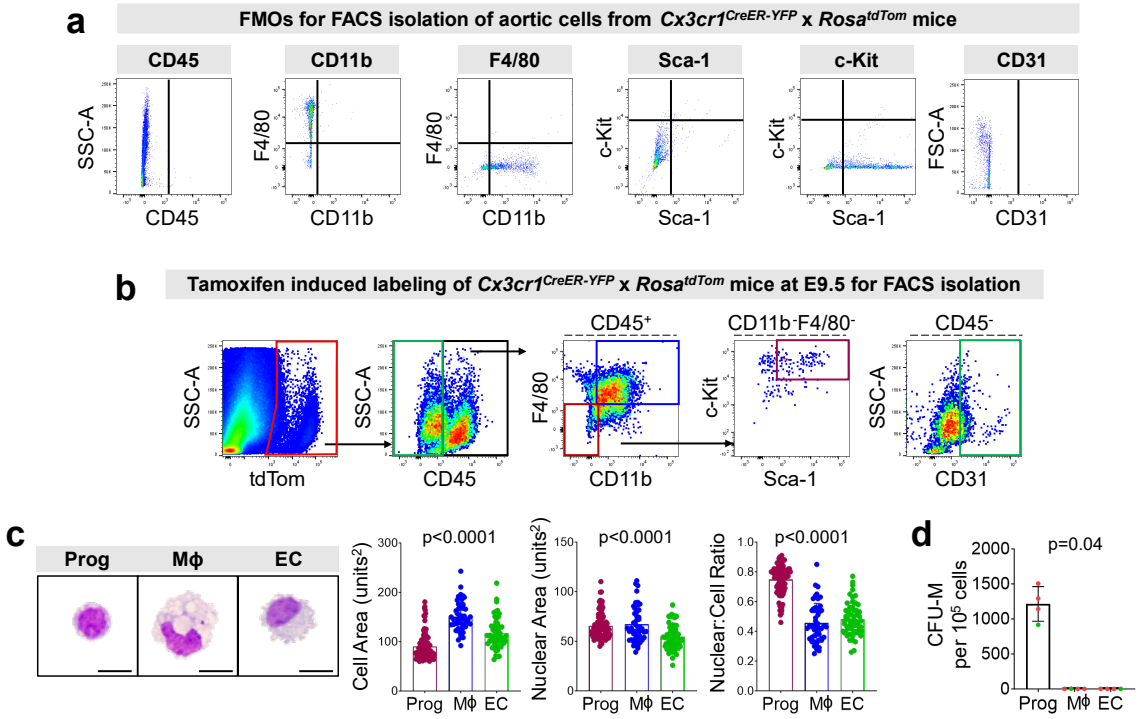

Supplementary Fig. 7. Embryonic CX3CR1^{+} cells give rise to EndoMac progenitors in postnatal aorta.

(a-d) *Cx3cr1*$^{CreER-YFP}$ x *Rosa*^{tdTom} mice were induced with tamoxifen (TAM) at E9.5 and aortas of 12 w offspring used for fluorescence assisted cell sorting (FACS) of tdTomato positive (tdTom^{+}) aortic cells.

(a) Fluorescence-minus-one (FMO) controls used to sort aortic cells.

(b) FACS-isolation of tdTom^{+} macrophages (Mϕ, blue), progenitors (Prog, maroon) and endothelial cells (EC, green) from 12 w aorta (n = 3 experiments using pooled aortas from ≥ 6 mice).

(c) Wright-Giemsa staining of sorted cell populations, and graphs showing comparison of total cell area, nucleus area and nucleus:cell area ratio (Prog: 100 cells, Mϕ: 51 cells and EC:59 cells). Data were analyzed using Kruskal-Wallis test with Dunn's multiple comparisons test. Adjusted p-values for cell area: $p < 0.0001$ Prog vs Mϕ and EC, and Mϕ vs

EC; nuclear area: $p < 0.0001$ Prog vs EC and $p = 0.0002$ Mϕ vs EC; nucleus:cell ratio: $p < 0.0001$ Prog vs Mϕ and EC.

(d) CFU-M yield from $tdTom^+$ (red dots) and GFP^+ (green dots) progenitors, macrophages and endothelial cells isolated from adult aortas of E9.5 TAM-induced *Cx3cr1*$^{CreER\text{-}YFP}$ x *Rosa*^{tdTom} mice and E8.5 TAM-induced *Csf1r*$^{Mer\text{-}iCre\text{-}Mer}$ x *Rosa*^{mTmG} mice, respectively ($n = 4$ experiments, using six aortas each). Friedman test.

Data summarized as mean ± SD.

Also see Fig. 3. Source data are provided as a Source Data file.

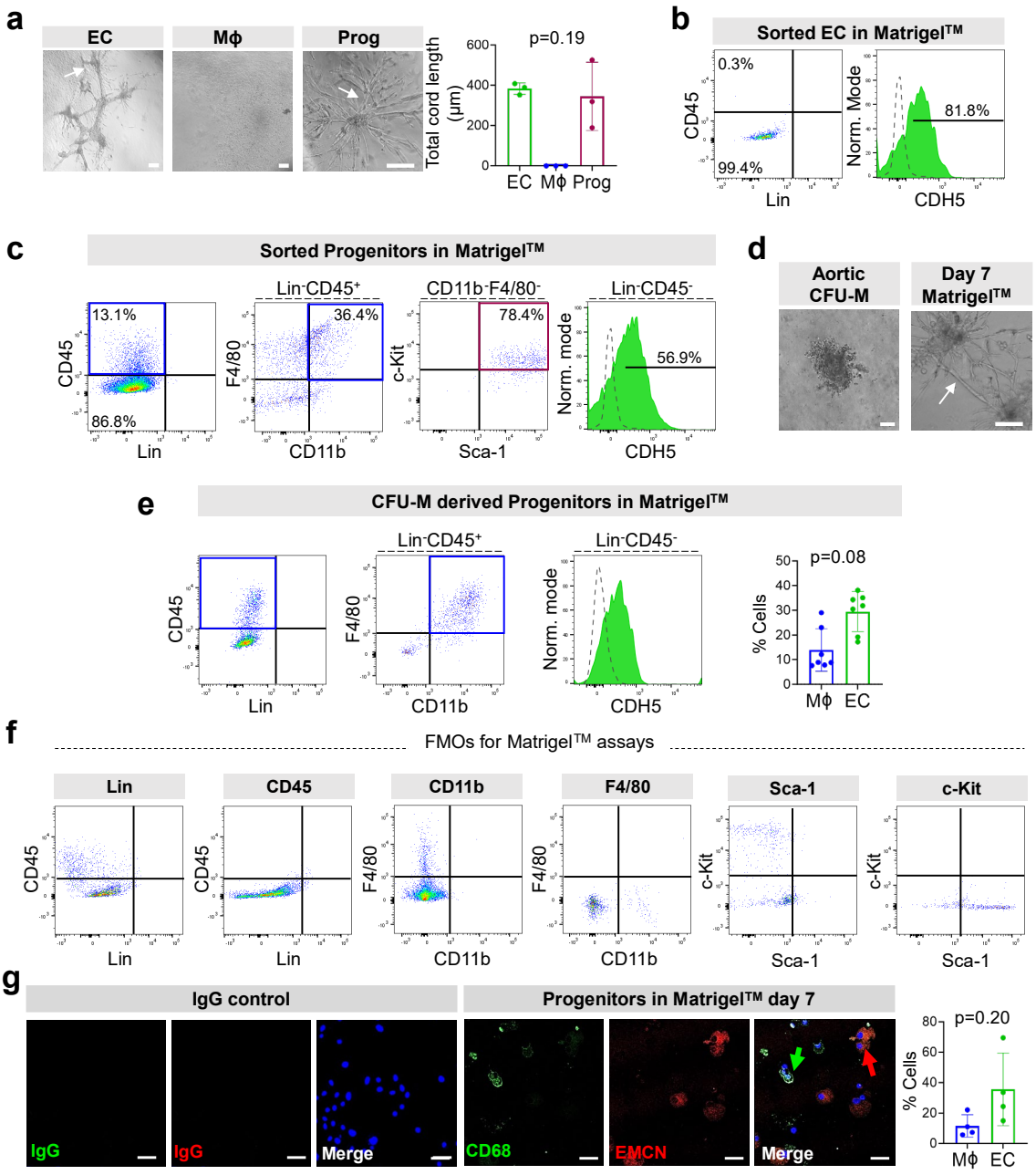

Supplementary Fig. 8. Aortic CFU-M progenitors have endothelial and macrophage differentiation potential.

(a) Light microscopy images of fluorescence assisted cell sorting (FACS)-isolated endothelial cells (EC), macrophages (Mϕ) or progenitors (Prog) from 12 w C57BL/6J aorta cultured in Matrigel™ for 7 days. Arrows indicate cords. Graph shows total cord length (n = 3 experiments, six aortas each; Friedman test).

(b, c) Flow cytometry plots and histograms showing the cell types produced from FACS-isolated primary aortic (b) endothelial cells and (c) progenitors after culture in Matrigel™ for 7 days (n = 1 experiment using aortas pooled from six mice). Green histogram, sample; dotted histogram, fluorescence-minus-one (FMO) control.

(d) Example of an aortic CFU-M (left) and branching cord networks produced from CFU-M derived progenitors in Matrigel™ at day 7 (right, arrow).

(e) Flow cytometry plots and graph show the cells produced from aortic CFU-M progenitors from adult C57BL/6J mice cultured in Matrigel™ for 7 days (n = 7 mice, three independent experiments; two-tailed Wilcoxon matched-pairs signed-rank test).

(f) FMO controls for (b), (c) and (e).

(g) Confocal microscopy of immunolabeled cytospin preparations of cells produced by CFU-M progenitors after culture in Matrigel™ for 7 days. Cells were immunolabeled for CD68 (green) and endomucin (EMCN; red), and nuclei stained with DAPI (blue). Graph summarises the percentage of $CD68^+$ and $EMCN^+$ cells (n = 4 independent experiments; two-tailed paired t-test).

Data summarized as mean ± SD. Scale bar, 40 μm in (a, d) and 100 μm in (g).

Also see Fig. 4. Source data are provided as a Source Data file.

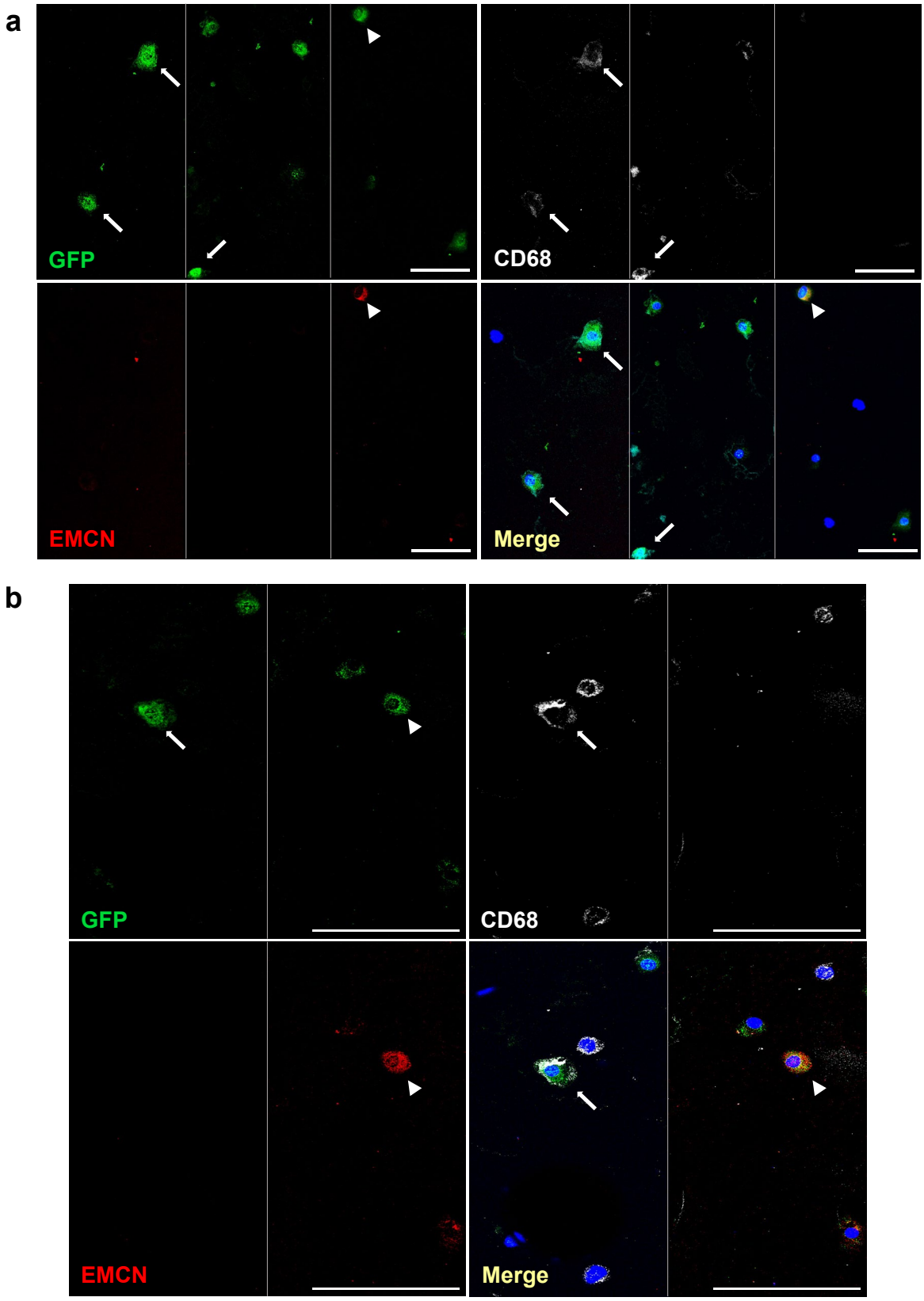

Supplementary Fig. 9. Aortic CFU-M progenitors are bipotent for endothelial cells and macrophages at a single cell level.

(a, b) A single GFP^+ aortic CFU-M progenitor cell was seeded with GFP^- progenitors on Matrigel™ in individual wells and cultured for 7 days. Cytospun preparations of resulting sprouts were immunolabeled as indicated. Confocal microscopy images of immunolabeled cells from two independent wells (a and b) show presence of GFP^+CD68^+ macrophages (arrows) and GFP^+EMCN^+ endothelial cells (arrowheads). $GFP^+CD68^-EMCN^-$ cells and GFP^-CD68^+ macrophages can also be seen. A montage of 2-3 fields of view per well is presented with white vertical lines demarcating the fields of view. Scale bar, 100 μm. Also see Fig. 4.

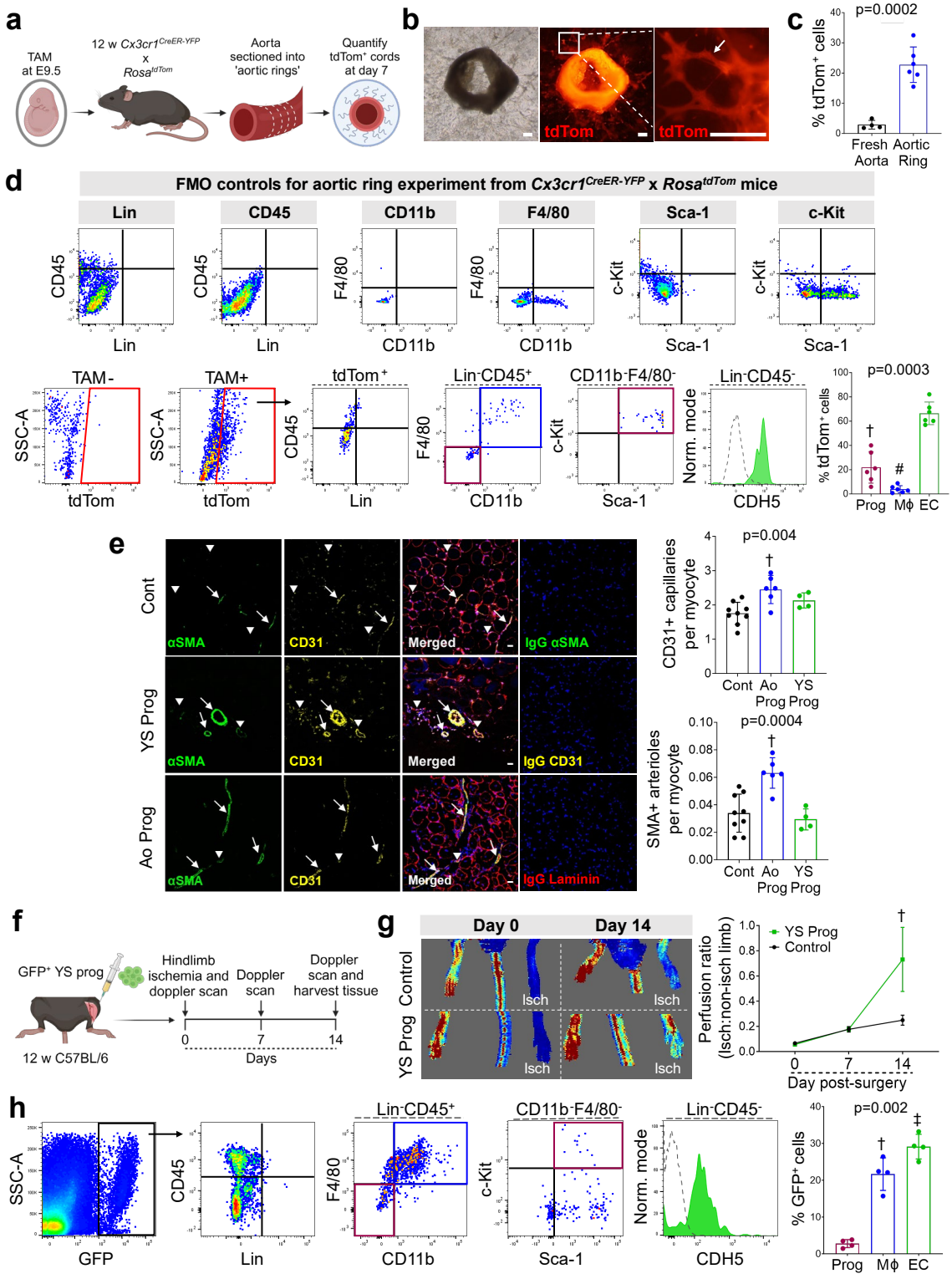

Supplementary Fig. 10. Endothelial and macrophage differentiation capacity of YS-derived progenitors.

(a) Schematic for aortic ring assay performed from aortas of E9.5 tamoxifen (TAM)-induced adult *Cx3cr1*$^{CreER\text{-}YFP}$ x *Rosa*^{tdTom} mice that express tdTomato (tdTom^{+}) in embryonically derived cells.

(b) Light and fluorescence microscopy images of an aortic ring showing tdTom^{+} adventitial sprouting.

(c) Graph comparing % tdTom^{+} expression in day 7 aortic ring assays with freshly digested aorta (aorta: 4 mice, aortic rings: 6 mice; two-tailed unpaired t-test).

(d) Flow cytometry of aortic ring assay sprouts from 12 w *Cx3cr1*$^{CreER\text{-}YFP}$ x *Rosa*^{tdTom} mice TAM-induced at E9.5. Top row: fluorescence-minus-one (FMO) controls. Bottom row: representative sample, with gated macrophages (Mϕ, blue), progenitors (Prog, maroon) and endothelial cells (EC, green histogram; dotted, FMO control). tdTom expression in no TAM (TAM^{-}) control also shown. Graph shows the composition of tdTom^{+} cells in aortic ring sprouts (n = 6 mice; repeated measures one-way ANOVA with Tukey's multiple comparisons test (†p = 0.008 and #p < 0.0001 vs EC).

(e) Confocal microscopy of immunolabeled sections of hindlimb muscle at day 14 after ischemia surgery and administration of Matrigel^{TM} (Cont, top) or E9.5 yolk sac (YS) CFU-M progenitors (YS Prog, middle) or aortic CFU-M progenitors (Ao Prog, bottom). Sections were immunolabelled for CD31 (yellow), αSMA (green), and laminin (red) for myocytes, and nuclei stained with DAPI (blue). IgG negative controls also shown. Graphs show capillary and arteriolar densities. Cont: 9, Ao Prog: 6 and YS Prog: 4 mice, three sections/mouse. Data analyzed using one-way ANOVA with Dunnette's (†p = 0.002 vs Cont) and Tukey's (†p = 0.0008 vs Cont) multiple comparisons test, respectively.

(f) Schematic of 1º transfer of GFP^{+} YS CFU-M progenitors into hindlimb muscle after ischemia surgery with 14 days follow-up.

(g) Laser Doppler perfusion images of mice on days 0 and 14 post-ischemia and administration of cell-free Matrigel^{TM} (Control, top) or YS progenitors (bottom). Graph shows results over time. $n \geq 4$ mice; mixed effects two-way ANOVA ($p = 0.0004$ for time, $p = 0.08$ for group, and $p = 0.02$ for time x group) with Sidak's multiple comparisons test (†$p = 0.003$ Prog vs control).

(h) Flow cytometry plots and graph show cells produced by GFP^{+} YS progenitors in recipient hindlimb muscle ($n = 4$ mice). Green histogram, sample; dotted, FMO control. Data analyzed using repeated measures one-way ANOVA with Tukey's multiple comparison test (†$p = 0.008$ and ‡$p < 0.0006$ vs Prog).

Data summarized as mean ± SD. Scale bar, 100 μm (b, e).

Also see Fig. 5. Source data are provided as a Source Data file.

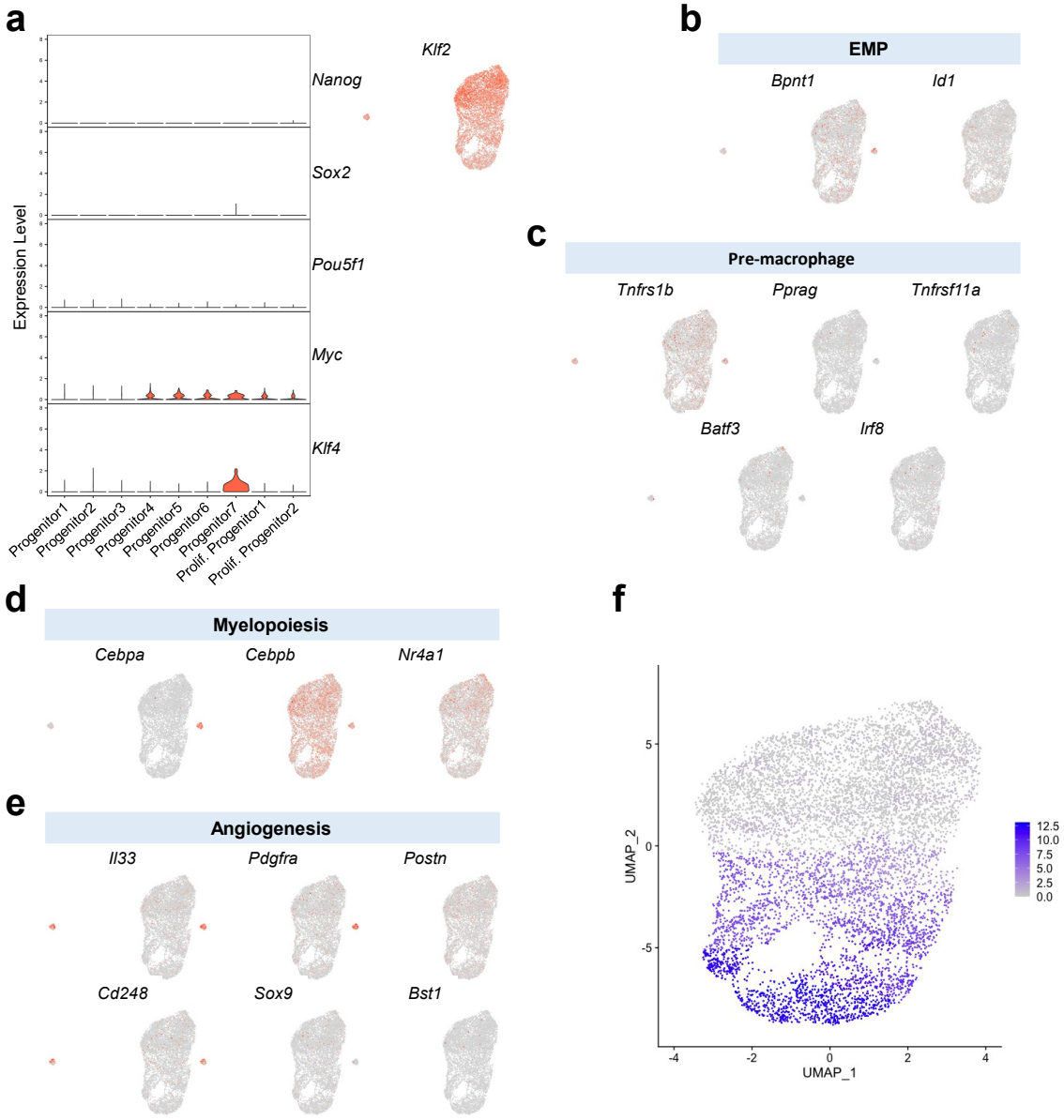

g

Cluster	Salient significantly overrepresented pathways
Prog 1	Immune system; long-term potentiation; EPO, NGF, VEGF, IL, MAPK and Notch signaling
Prog 2	Protein translation; immune system; IL and cytokine -cytokine receptor signaling
Prog 3	Immune system; Rho GTPases, MAPK, NGF, TGF -beta and TGFBR signaling
Prog 4	Protein synthesis, metabolism and targeting; mitochondrial energy production
Prog 5	Gene expression; mitotic cell cycle; mitochondrial energy production
Prog 6	Mitochondrial energy production; mitotic cell cycle, protein synthesis; adaptive immune system
Prog 7	ECM organization and degradation; ECM-cell interaction; VEGF signaling
Prolif. Prog 1	mitotic cell cycle; mitochondrial energy production; apoptosis
Prolif. Prog 2	mitotic cell cycle; mitochondrial energy production; apoptosis; immune system

Supplementary Fig. 11. Aortic CFU-M progenitors exhibit a myelopoietic and

vasculogenic transcriptional profile with a continuum of cell states.

Aortic CFU-M progenitors cultured from two adult C57BL/6J mice were pooled and viable cells analyzed by scRNA-seq.

(a) Violin plots illustrate cluster-wise expression of selected stem cell genes (left) and UMAP plot overlaid with expression of *Klf2* (right) showing cell specificity of expression.

(b-e) Expression levels of the indicated marker genes for (b) erythromyeloid progenitors (EMPs), (c) pre-macrophages, (d) myelopoiesis and (e) angiogenesis, overlaid on the UMAP plot showing cell specificity of expression.

Expression levels in (a)-(e) are shown as log normalized counts. The gray to red gradient in (b-e) represents low to high expression.

(f) UMAP plot showing trajectory analysis of single cells in pseudotime. Cells are colored by pseudotime. The analysis shows progression of cell states from cluster 1 at the top to proliferative clusters at the bottom. The Monocle3 algorithm identified Cluster 7 as a separate partition, thus it was not included in the analysis.

(g) The table lists the notable overrepresented pathways in the assigned cell clusters. Pathway analysis was performed using InnateDB. Prog, progenitors; Prolif, proliferative; EPO, erythropoietin; NGF, nerve growth factor; VEGF, vascular endothelial growth factor; IL, interleukin; MAPK, mitogen activated protein kinase; GTP, Guanosine-5'-triphosphate; TGF, transforming growth factor; TGFBR, transforming growth factor-beta receptor; ECM, extracellular matrix.

Also see Fig. 6.

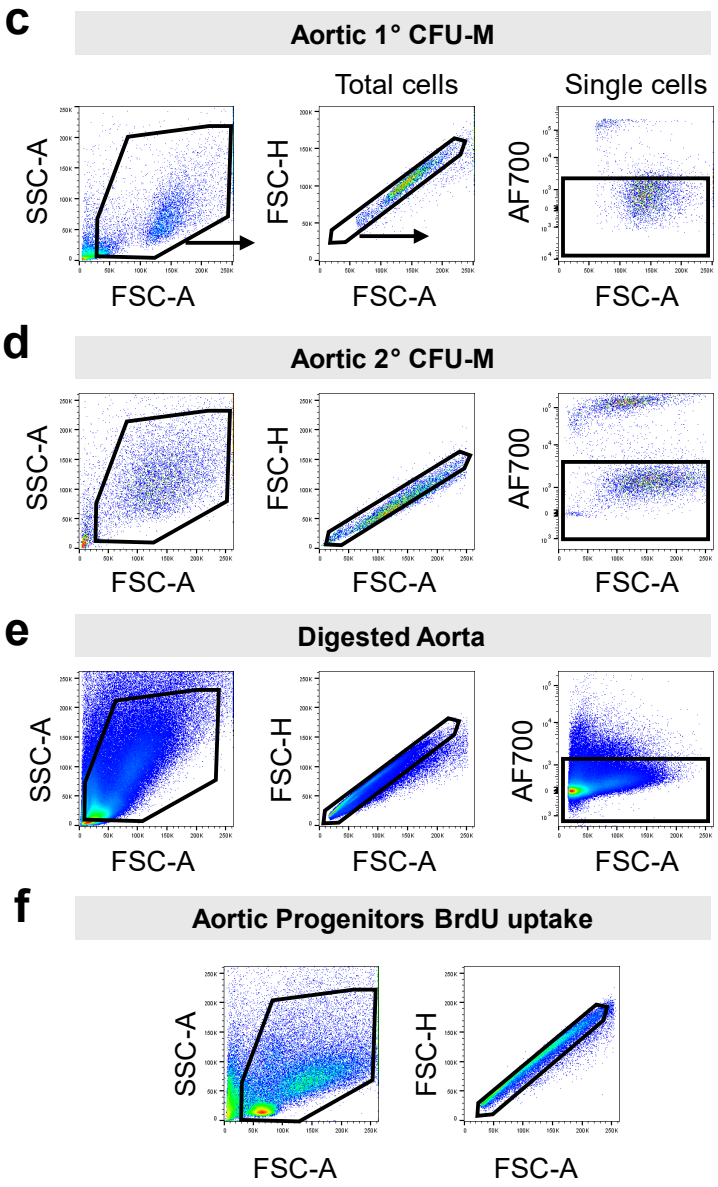

Supplementary Fig. 12. Gating strategies used for analysis of flow cytometry data shown in Fig. 1. Panels correspond to those in Fig. 1. Gating strategy in panel (c) was also used to analyze data presented in Supplementary Fig. 1b.

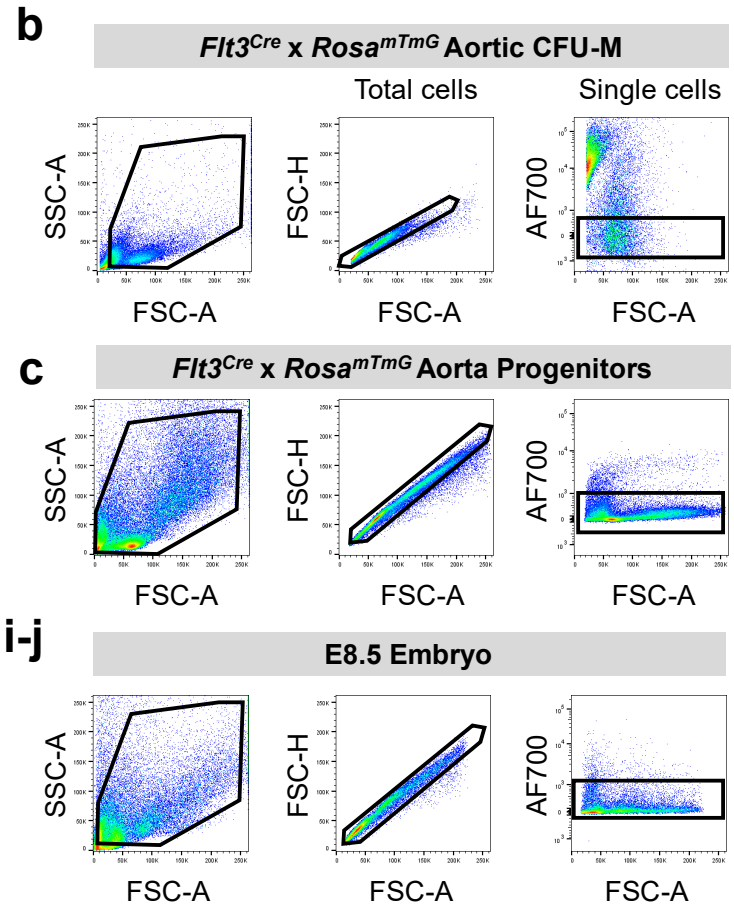

Supplementary Fig. 13. Gating strategy used for analysis of flow cytometry data presented in Fig. 2. Panels correspond to those in Fig. 2.

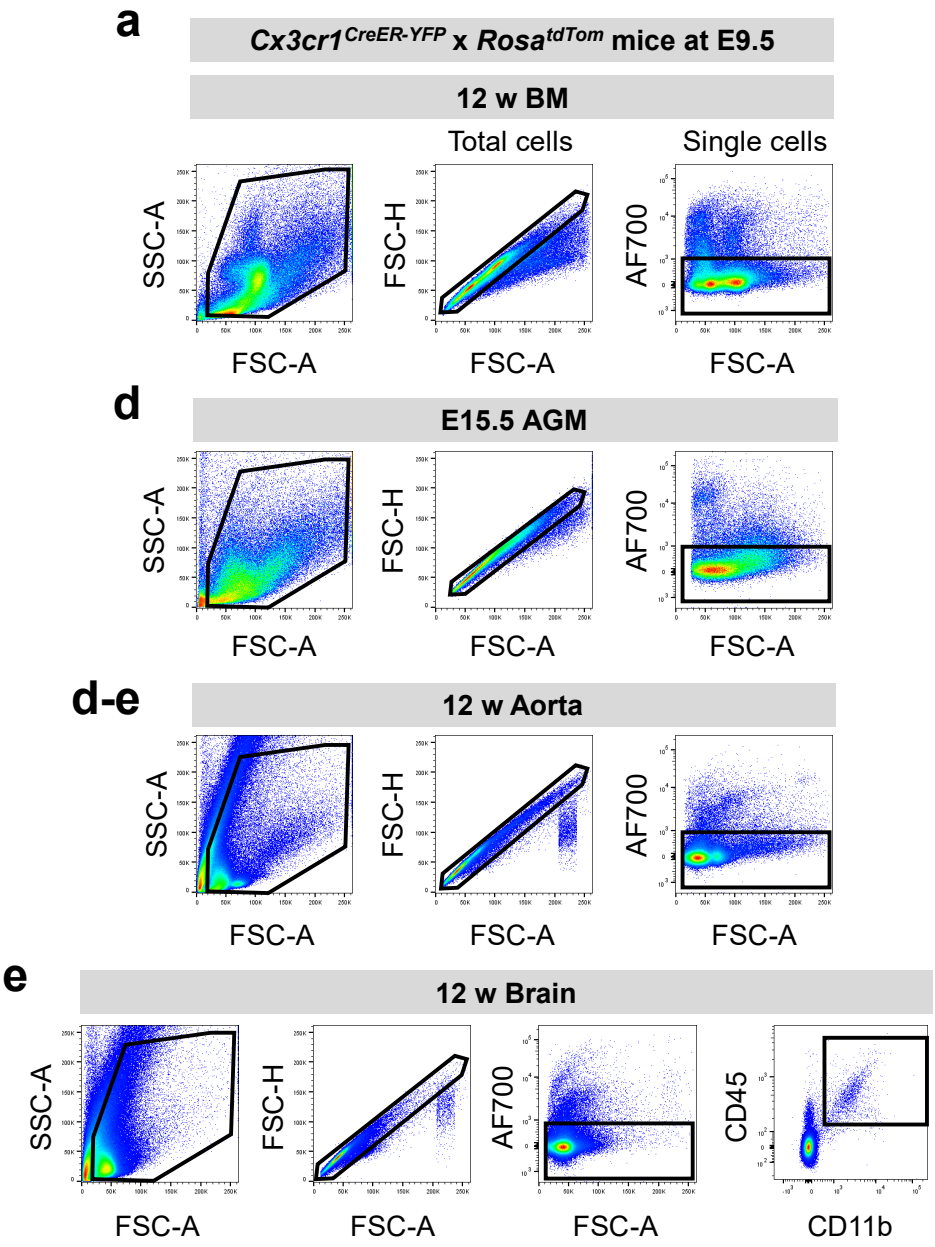

Supplementary Fig. 14. Gating strategies applied for analysis of flow cytometry data shown in Fig. 3a, 3d and 3e. Panels correspond to those in Fig. 3.

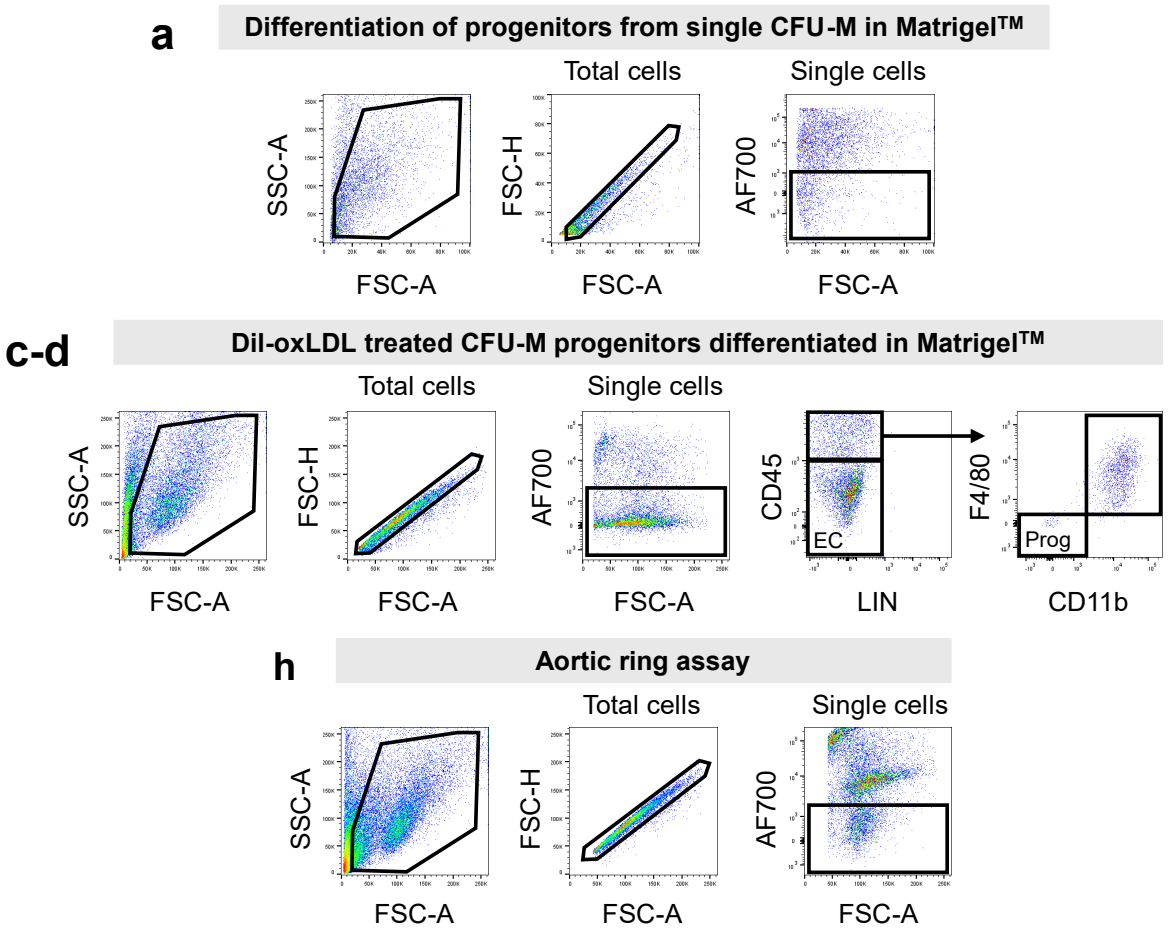

Supplementary Fig. 15. Gating strategies utilized to analyze the flow cytometry data presented in Fig. 4. Panels correspond to those in Fig. 4.

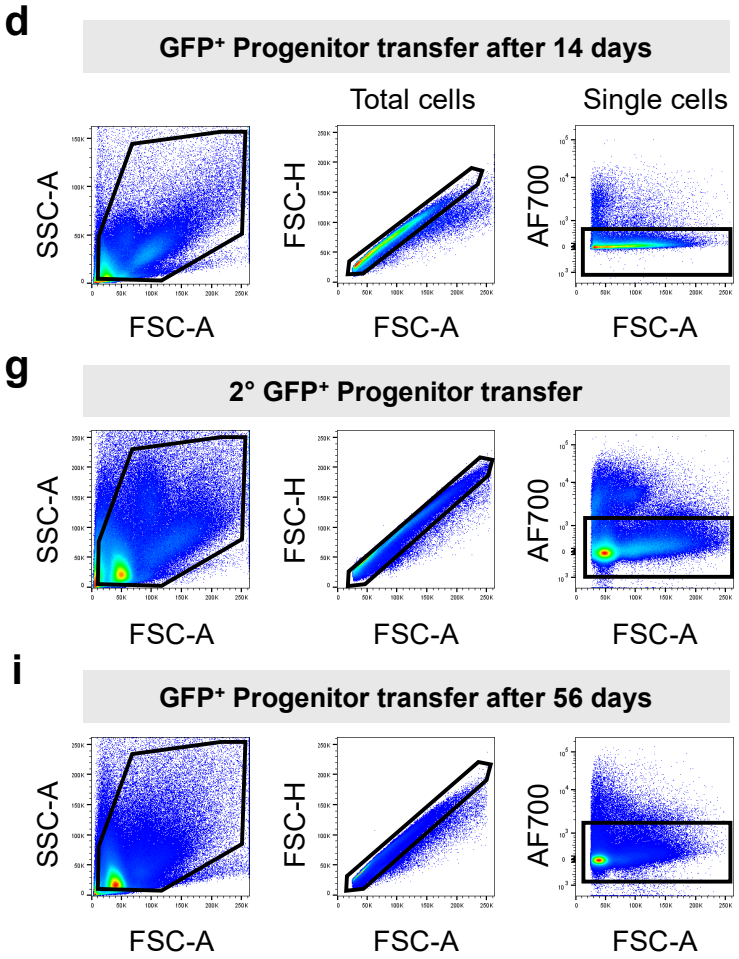

Supplementary Fig. 16. Gating strategy used for analysis of flow cytometry data from adoptive transfer experiments in mouse model of hindlimb ischemia shown in Fig. 5.

Panels correspond to those in Fig. 5.

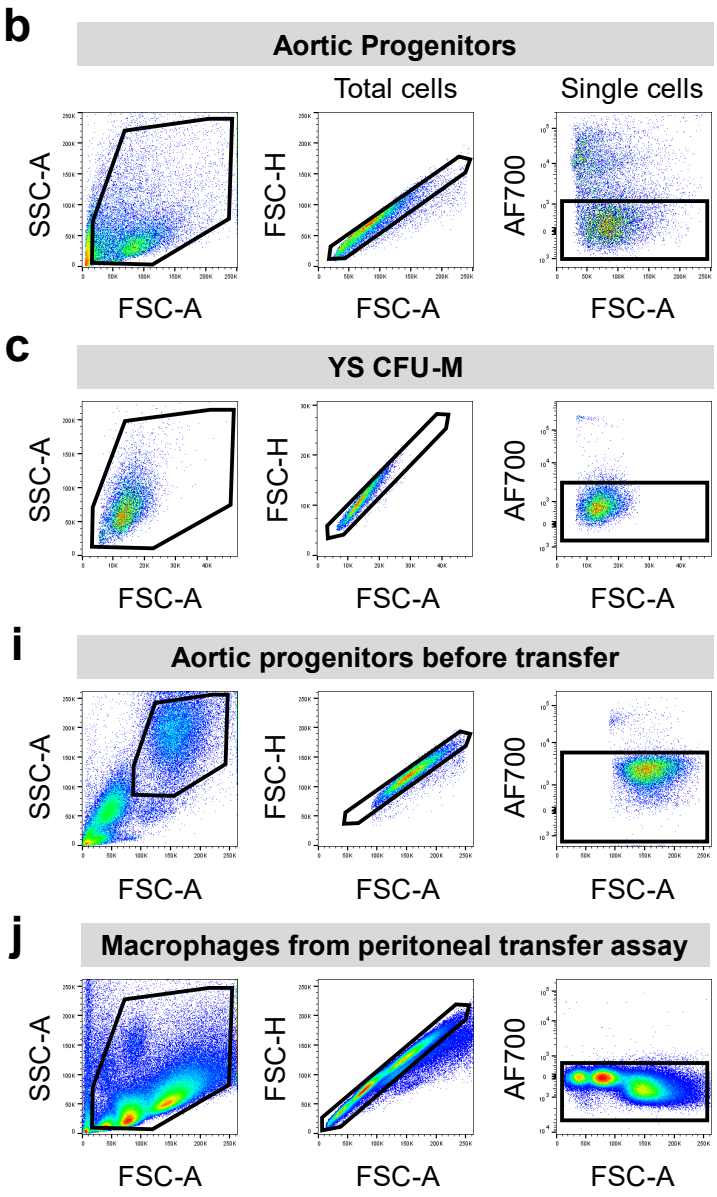

Supplementary Fig. 17. Gating strategy used for analysis of flow cytometry data presented in Fig. 7. Panels correspond to those shown in Fig. 7. Gating strategy for Fig. 7a is shown in Supplementary Fig. 12c.

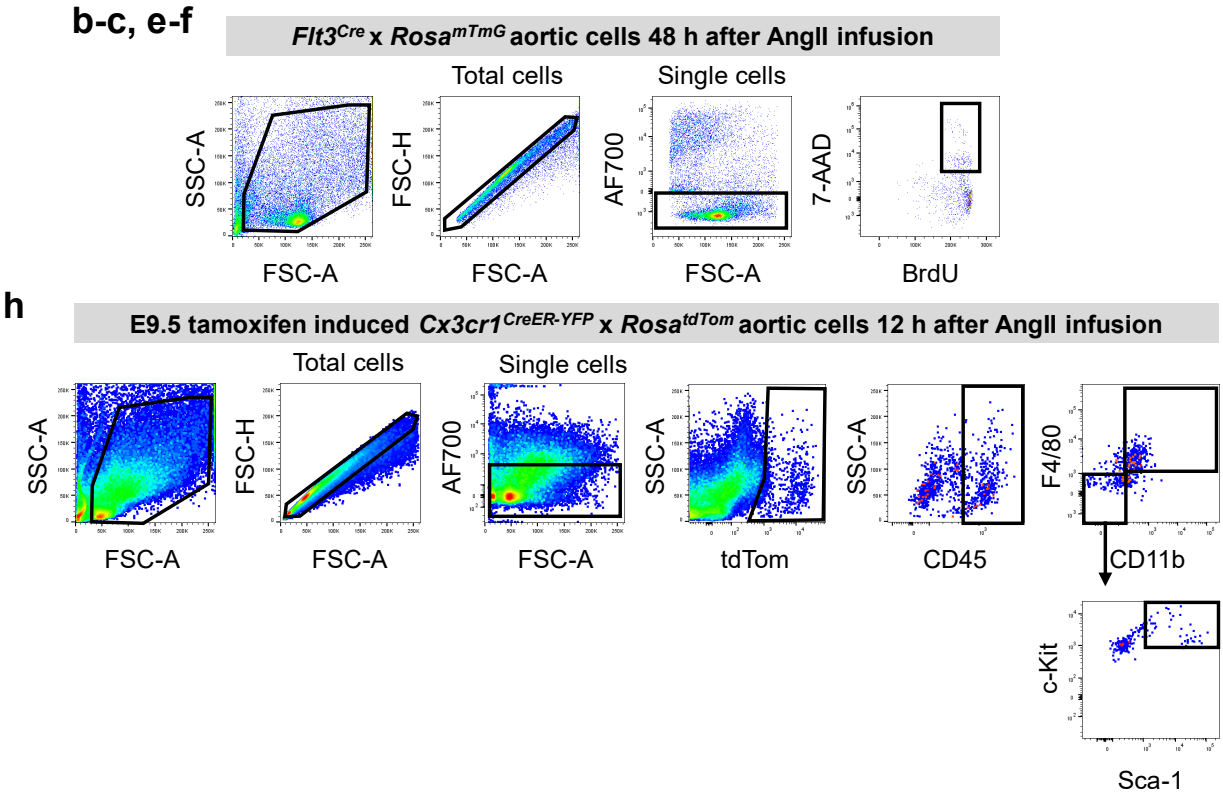

Supplementary Fig. 18. Gating strategies employed for analysis of flow cytometry data presented in Fig. 8. Panels correspond to those shown in Fig. 8.

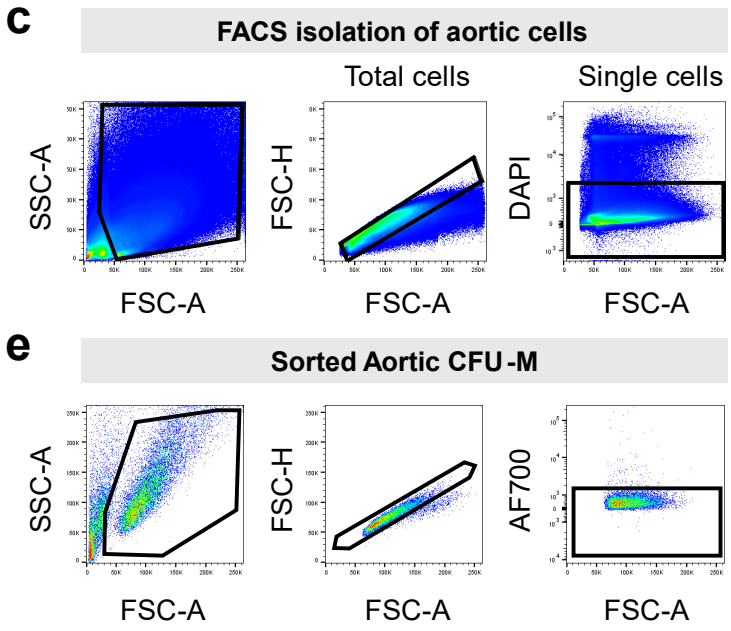

Supplementary Fig. 19. Gating strategy used for analysis of flow cytometry data shown in Supplementary Fig. 2. Panels correspond to those in Supplementary Fig. 2.

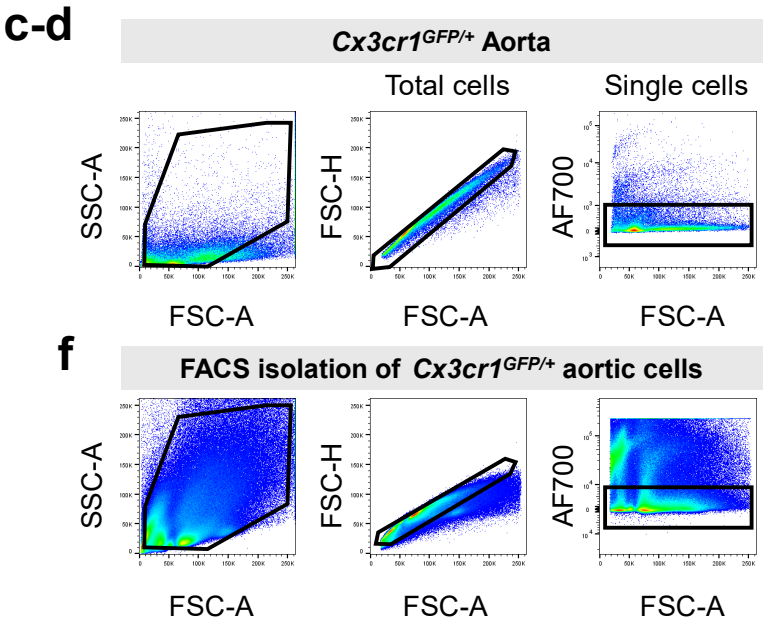

Supplementary Fig. 20. Gating strategy used to analyze the flow cytometry data presented in Supplementary Fig. 3. Panels correspond to those in Supplementary Fig. 3.

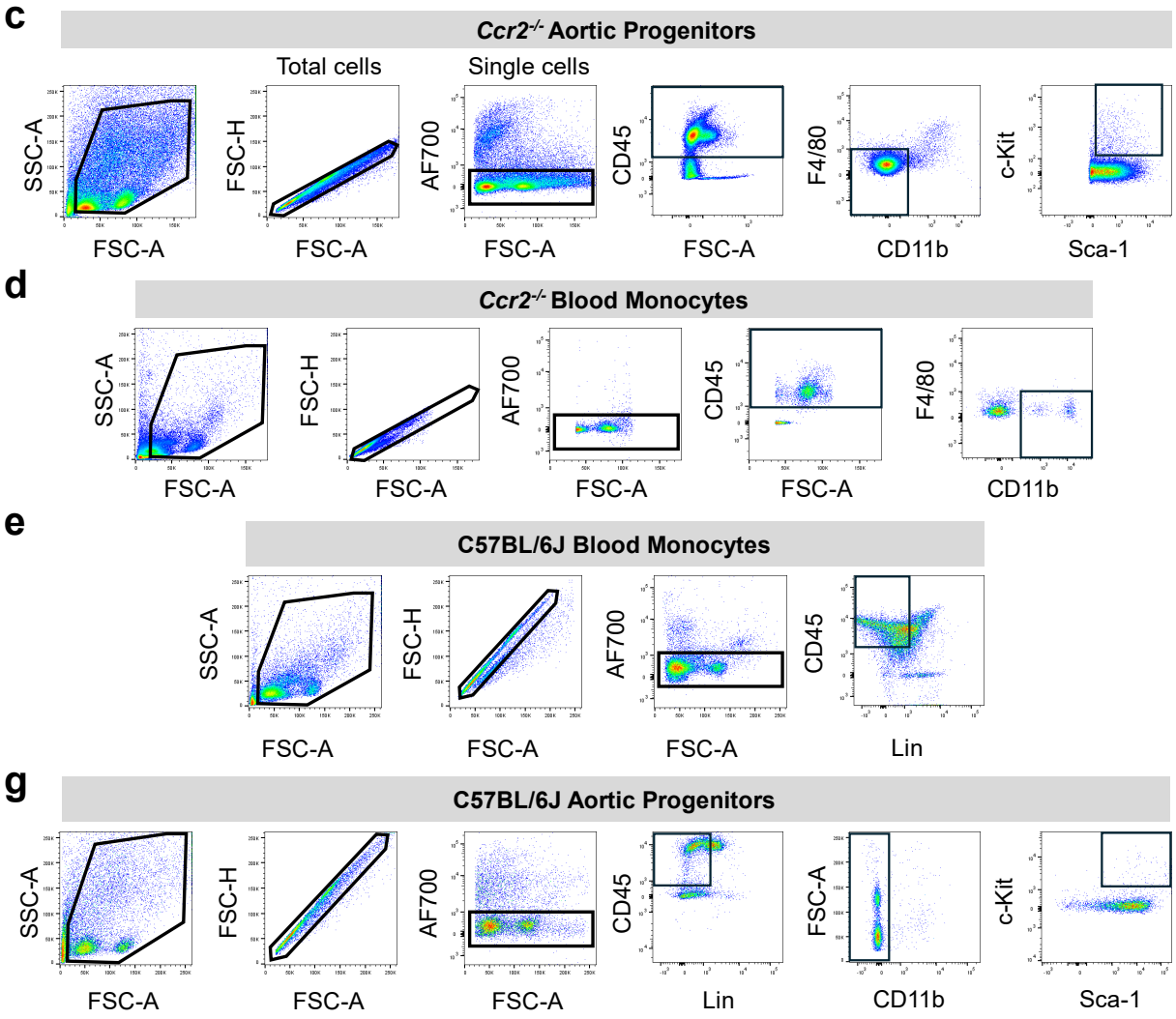

(Contd. on next page)

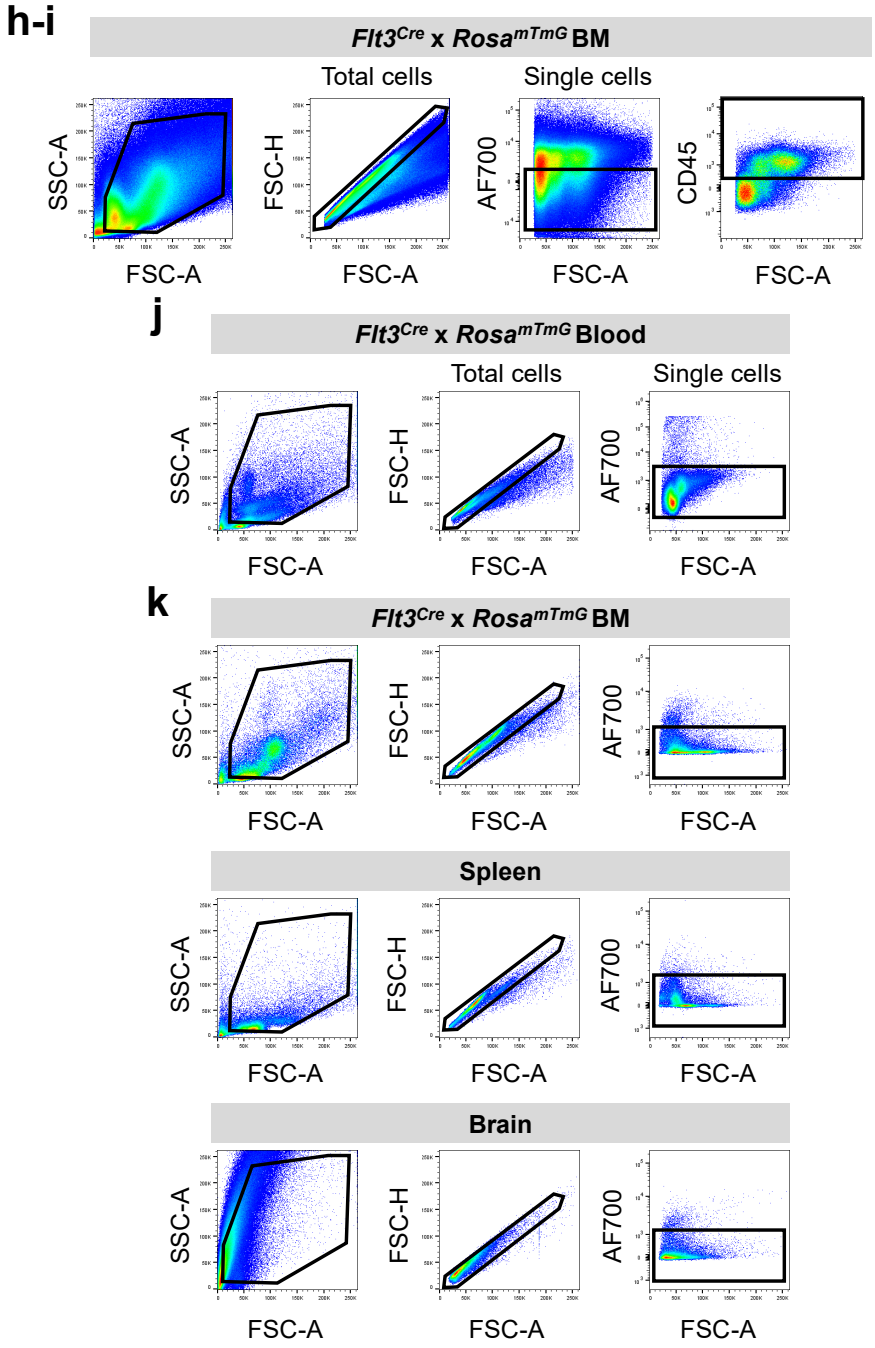

Supplementary Fig. 21. Gating strategies employed for analysis of flow cytometry data presented in Supplementary Fig. 4. Panels correspond to those in Supplementary Fig. 4. Gating strategy for analysis of aortic cells in Supplementary Fig. 4k is shown in Supplementary Fig. 13c.

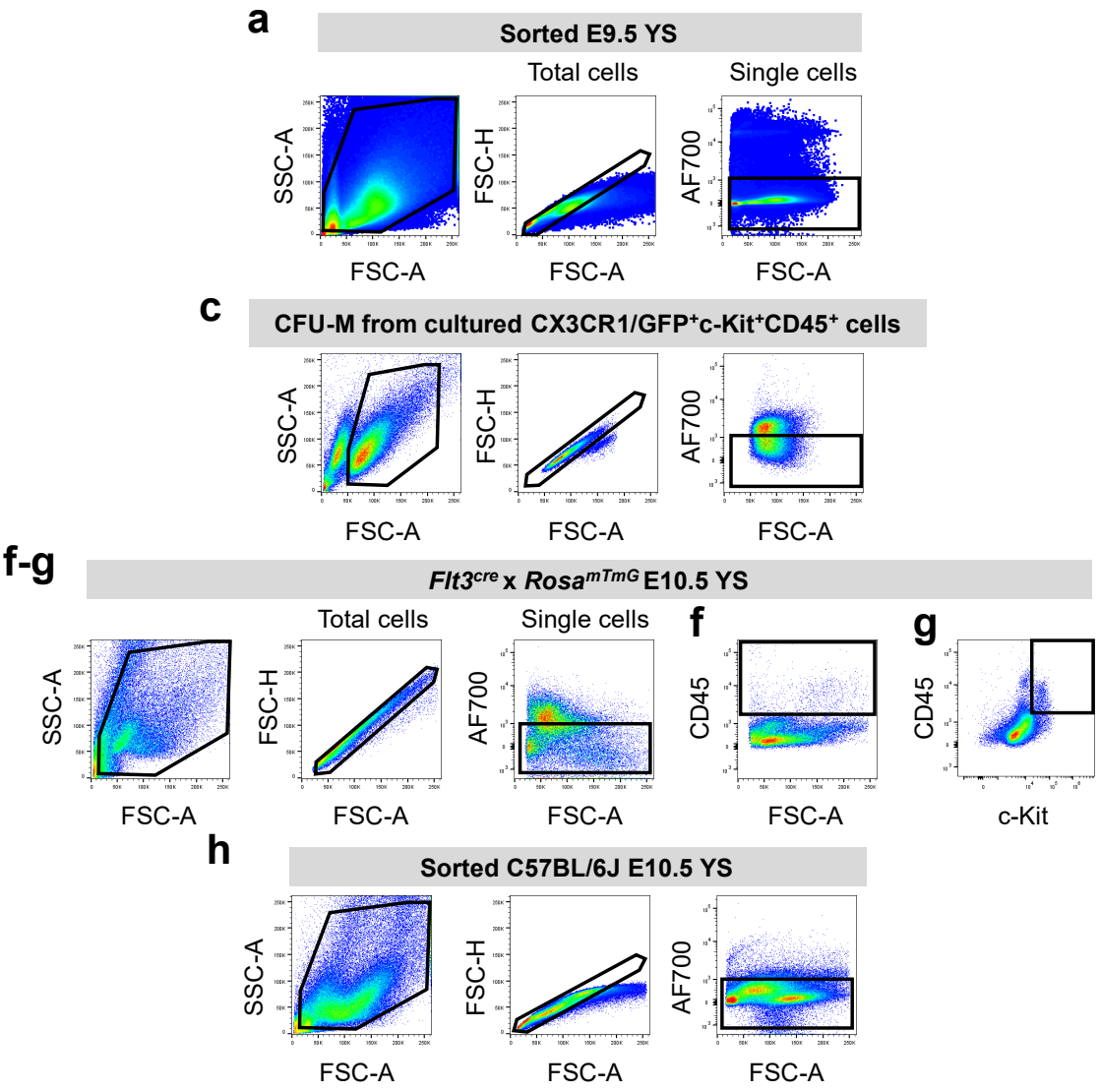

Supplementary Fig. 22. Gating strategies used for analysis of flow cytometry data shown in Supplementary Fig. 5. Panels correspond to those shown in Supplementary Fig. 5.

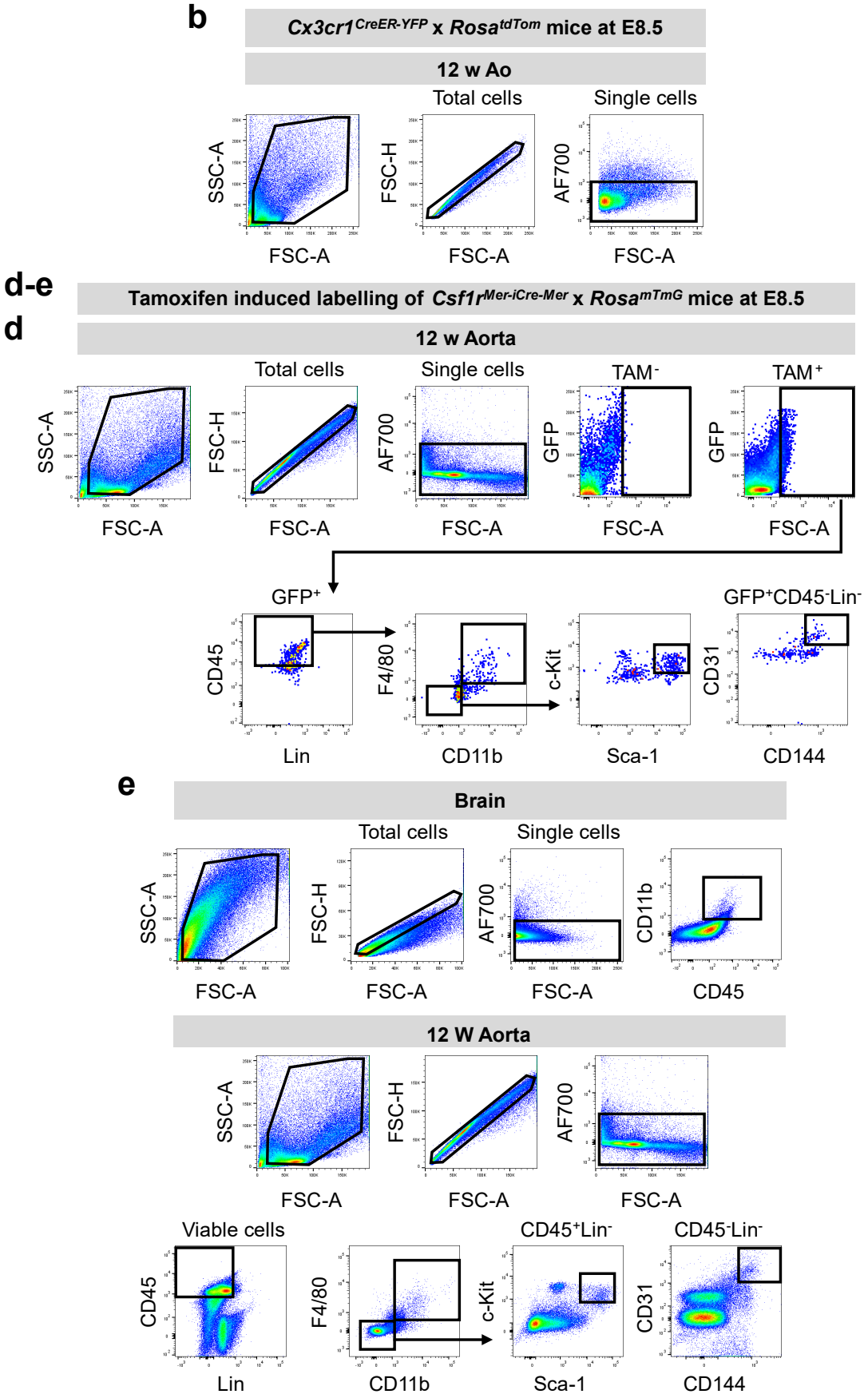

Supplementary Fig. 23. Gating strategies utilized for analysis of flow cytometry data

presented in Supplementary Fig. 6. Panels correspond to those shown in Supplementary Fig. 6.

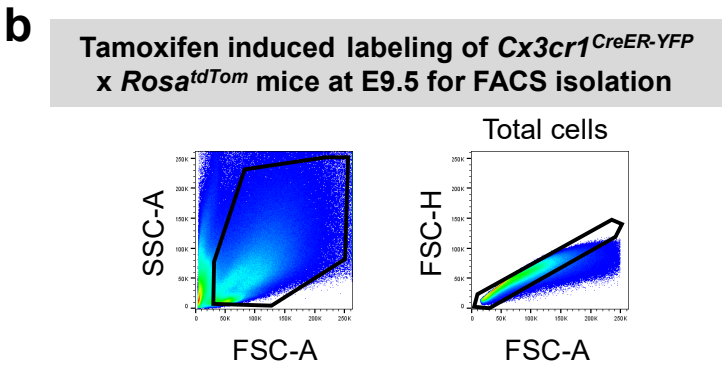

Supplementary Fig. 24. Gating strategy used to analyze the flow cytometry data presented in Supplementary Fig. 7b. Panel corresponds to that in Supplementary Fig. 7.

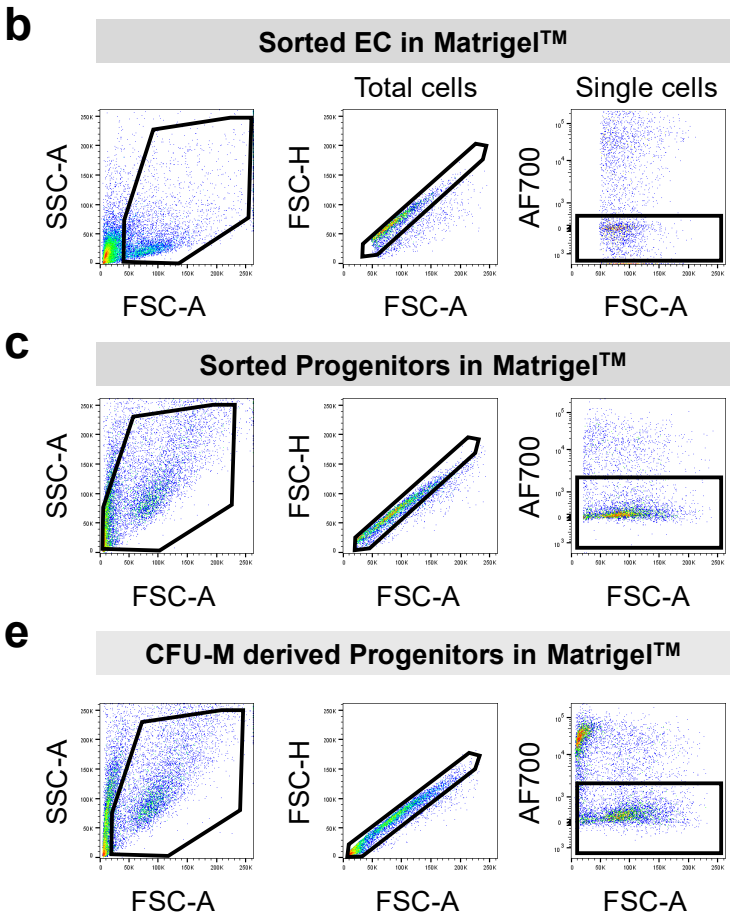

Supplementary Fig. 25. Gating strategy used for analysis of flow cytometry data presented in Supplementary Fig. 8. Panels correspond to those in Supplementary Fig. 8.

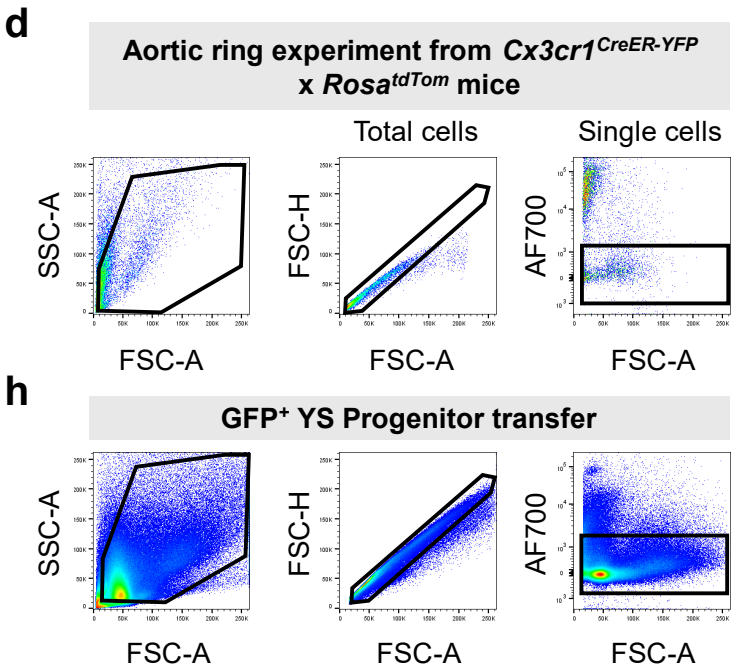

Supplementary Fig. 26. Gating strategy used to analyze the flow cytometry data presented in Supplementary Fig. 10. Panels correspond to those in Supplementary Fig. 10.